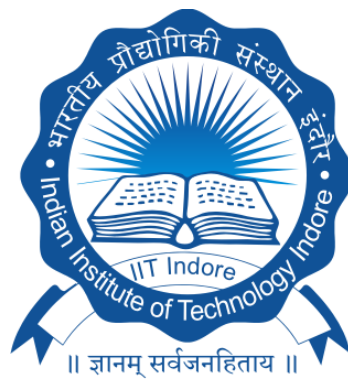


MWA investigation of pulsar emission characteristics and single-pulse properties

M.Sc. Project

By

Hemanth Bommireddy



Discipline of Astronomy, Astrophysics and Space Engineering

INDIAN INSTITUTE OF TECHNOLOGY INDORE

June 12, 2021

MWA investigation of pulsar emission characteristics and single-pulse properties

M.Sc.Project

*Submitted in partial fulfillment of the
requirements for the awards of the degree
of
Master of Science*

by

Hemanth Bommireddy



Discipline of Astronomy, Astrophysics and Space Engineering

INDIAN INSTITUTE OF TECHNOLOGY INDORE

June 12, 2021



INDIAN INSTITUTE OF TECHNOLOGY INDORE

CANDIDATE'S DECLARATION

I hereby certify that the work which is being presented in the thesis entitled '**MWA investigation of pulse emission characteristics and single pulse properties**' in the partial fulfillment of the requirements for the award of the degree of **MASTER OF SCIENCE** and submitted in the **Department of Astronomy, Astrophysics and Space Engineering, Indian Institute of Technology Indore**, is an authentic record of my own work carried out during the time period from 25/July/2019 to 09/June/2021. Thesis submission under the supervision of **Dr. Manoneeta Chakraborty**, Assistant Professor.

The matter presented in this thesis has not been submitted by me for the award of any other degree of this or any other institute.

Hemanth
9/6/21

Signature of the student with date
(Hemanth Bommireddy)

This is to certify that the above statement made by the candidate is correct to the best of my knowledge.

Manoneeta Chakraborty

09/06/2021

Signature of the Supervisor of M.Sc. thesis (with date)
MANONEETA CHAKRABORTY

Hemanth Bommireddy has successfully given his M.Sc. Oral Examination held on **09/06/2021**.

Manoneeta Chakraborty

Signature(s) of Supervisor(s) of MSc thesis
Date: 09/06/2021

Suman Majumdar
10/06/2021

Convener, DPGC
Date:

Saptarshi Ghosh

Signature of PSPC Member #1
Date: 10/06/2021

Dr. Manoneeta Chakraborty

Signature of PSPC Member #2
Date: 10/06/2021

S. Das

Signature of PSPC Member #3
Date: 10/06/2021

Shubha

Signature of M.Sc coordinator
Date: 10-06-2021

Abhishek

Signature of Head of the department
Date: 10/06/2021

ACKNOWLEDGEMENTS

I would like to express my sincere gratefulness to my supervisor **Dr. Manoneeta Chakraborty** , for giving me the opportunity to work with her and also for providing excellent guidance, encouragement, moral support and continuous assistance throughout this project and also for his patience, motivation and enthusiasm for helping me to complete this work.

I also wish to express my deep sense of gratitude to **Ms. Parul Janagal** for her active collaboration in this project and for her insightful suggestions and discussion at the time of need.. I would also like to thank my PSPC members Dr.Bhargav Vaidya, Dr. Saurabh Das and Dr. Saptarshi Ghosh for their invaluable scrutiny and feedback on my project at regular intervals and under various formal and informal settings.

I also acknowledge the essential facilities, specifically the computing facilities in which most of the data analysis related to this project was done, provided by the DAASE at IIT Indore.

Lastly,I would like to thank my mother (Mrs. Satya Vani), father(Mr. Bhaskar Reddy), who have supported me through out this research work.

Abstract

Periodic sub-pulse modulation in pulsars, where intensity of sub-pulses modulate periodically, is still an unexplained phenomenon. Its evolution needs to be studied to understand characteristics of periodic pulse modulations and associated features like nulling, drifting, etc., observed in a large sample of pulsars. We explore the pulse and single-pulse observations of the pulsar PSR J1825–0935 obtained using the Murchison Widefield Array (MWA) with a central frequency of 184.96 MHz. Our analysis of these unprecedented high sensitivity observations at these frequencies reveal the low frequency behavior of the single-pulse periodic intensity modulations from PSR J1825–0935 . In future, we plan to examine this behavior at different epochs and correlate with the physical parameters of the pulsar to shed light on its emission mechanism, especially at low frequencies.

Contents

List of Figures	i
List of Tables	iii
Acronyms	iii
1 Introduction	1
1.1 Neutron stars and Pulsars	1
1.1.1 Pulsar discovery and basic properties	2
1.1.2 Observing pulsars	4
1.1.3 Motivation	5
1.1.4 Emission Mechanism	6
1.1.5 Emission properties	6
1.1.6 Within these pulses	7
1.1.6.1 Nulling	8
1.1.6.2 Drifting subpulses	8
1.1.6.3 Periodic Amplitude Modulations	8
2 Murchison Widefield Array (MWA)	12
2.1 Role of MWA in pulsars study	13
3 Source and observation	15
3.1 Source	15
4 Methodology and Results	18
4.1 PRESTO	18
4.2 DSPSR	20
4.3 Binning	21
4.4 Pulse profile	21
4.5 Pulse stack	23

4.6	Modulation Index	24
4.6.1	LRFS	26
4.7	Pulse energy	28
4.7.1	Pulse energy studies - epoch I	30
4.7.2	Pulse energy studies - epoch II	31
4.7.3	Pulse energy distribution	34
4.7.4	Polarisation analysis	36
5	Discussion and conclusion	38
6	Future Plans	42

List of Figures

1.1	Model of rotating neutron star [9].	3
1.2	The dispersion effect to progressive delay in pulses at different frequencies [9].	5
1.3	A sample of pulse profiles showcasing their varying nature and complex structure between different sources (a, b, c, d, f, h). The time evolution of the profile can also be observed often for the same pulsar as shown by e, g, and h [9].	7
1.4	Emission models	8
1.5	Comparison of periodic characteristics of radio pulsars [3].	10
1.6	Distribution of modulation periodicity with spin-down energy \dot{E} for various pulsars [3].	10
1.7	The left panel shows distribution of modulation periodicity in units of the pulsar period P and right panel distribution of spin-down energy for drifting and other sub-pulse modulations [3].	11
2.1	Array of dipole antennas- MWA [8].	12
2.2	MWA configuration [8]	14
3.1	Mean pulse profile of PSR J1825-0935 [1].	15
4.1	Flow chart of data flow for obtaining pulsar candidates [9].	19
4.2	Folded pulse profile plot of PSR J1825–0935 for 200 s observation time generated using PRESTO	19
4.3	Format of data in DSPSR [14]	20
4.4	Averaged pulse profile from PSR J1825–0935 computed over the entire 3500 s (epoch I). The strong main pulse can be very clearly seen, however no strong evidence of any interpulse is present.	22
4.5	Averaged pulse profile from PSR J1825–0935 computed over the entire 6500 s (epoch II). The strong main pulse can be very clearly seen, however a very weak indication of an interpulse can be observed.	22
4.6	10 binned pulse stack from PSR J1825–0935 computed over the entire 3500 s in epoch I. Variation in the strength of the pulse signal can be clearly seen in this plot.	23

4.7	10 binned pulse stack from PSR J1825–0935 computed over the entire 6500 s in epoch II. Variation in the strength of the pulse signal can be clearly seen in this plot.	24
4.8	Modulation Index of amplitude variation across the pulse profile of PSR J1825–0935 for epoch I. The green solid line shows the pulse intensity, the red solid line represents the standard deviation and the blue circles represents the modulation index.	25
4.9	Modulation Index of amplitude variation across the pulse profile of PSR J1825–0935 for epoch II. The green solid line shows the pulse intensity, the red solid line represents the standard deviation and the blue circles represents the modulation index.	25
4.10	LRFS of PSR J1825–0935 for whole epoch I, taking blocks of 512 length FFT	27
4.11	LRFS of PSR J1825–0935 for whole epoch II, taking blocks of 512 length FFT	27
4.12	Pulse energy variation across whole time of observation of PSR J1825–0935 for epoch I	29
4.13	Pulse energy variation across whole time of observation of PSR J1825–0935 for epoch II	29
4.14	Sliding FFT method applied to the non-stationary pulse energy vs. pulse number series for epoch I.	30
4.15	Power spectrum of the pulse energy region 800-1400	31
4.16	Pulse energy vs pulse number with 10 pulse averaging for epoch II. The orange solid line shows the Gaussian filter convolution of the underlying pulse energy plot.	32
4.17	Pulse energy vs pulse number trend for epoch II resulting from convolution with Gaussian filter. Here the high and the low pulse strength regions are shown with divisions using the black vertical lines.	33
4.18	Sliding FFT method applied to the non-stationary pulse energy vs. pulse number series for epoch II.	33
4.19	ON (blue curve) and OFF (orange curve) pulse energy distribution of PSR J1825–0935 for epoch I	34
4.20	ON (blue) and OFF (red) pulse energy distribution of PSR J1825–0935 for whole epoch II. The inset shows zoomed off pulse energy distribution. The variation on the on pulse distribution is significantly higher than the variation of the off pulse distribution in this case compared to epoch I.	35
4.21	Polarisation profile of PSR J1825–0935 for a section of epoch I	36
4.22	Polarisation profile of PSR J1825–0935 for whole epoch II	37
5.1	The pulse amplitude modulation parameters of pulsars B1055-52, B1702-19, B1822-09, and B1929+10 [1, 31, 32]. This table was taken from [25].	40

List of Tables

3.1	Details of the MWA observation of PSR J1825–0935 used for single-pulse analysis(Epoch I).	17
3.2	Details of the MWA observation of PSR J1825–0935 used for single-pulse analysis(Epoch II).	17

Chapter 1

Introduction

1.1 Neutron stars and Pulsars

Neutron stars are stellar remnants formed from supernovae explosion following the collapse of a main-sequence star after it stops nuclear fusion at its core. Stars having masses around 8 to 20 M_{\odot} generally form neutron stars, less than that mass white dwarfs are formed, and greater than that black holes are believed to be formed. Basic idea is that when a star fuses all the way to form iron, it has the highest binding energy at low pressure. Any further fission or fusion requires energy input which is not favourable. When the core mass is beyond 1.4 M_{\odot} , the electron degeneracy is overcome by gravity, so it energetically facilitates the production of neutrons and neutrinos from coalescing of protons and electrons. These neutrinos scatter and escape. Thus helping supernova happen, leaving a remnant where the neutron degeneracy is balancing the inward gravity force.

This collapse leaves behind the most dense objects with densities reaching order of nuclear densities and beyond that. They generally have a mass around 1.4 M_{\odot} and a radius of 10 km, with strong magnetic field from about 10^4 to 10^{11} Tesla (as a result of flux conservation during stellar collapse). Due to conservation of angular momentum, decrease in size of star results in an increase of rotation speed.

Pulsars are a special class of neutron stars. They spin very quickly, with the spin periods ranging from milliseconds to seconds. Their high

magnetic fields (10^8 to 10^9 Tesla) in presence of high rotation speeds leads to production of radio waves from its poles (as discussed in further sections) in a beamed fashion almost like a flash light. Since these objects were normal stars once upon a time, they are present throughout the galaxy. In order to observe these pulsars, proper orientation of pulsars towards earth is necessary. Depending on the orientation of the pulsars towards Earth, the pulse emission mechanism, and the misalignment of rotation and magnetic axis a variety of pulse profiles can be observed.

1.1.1 Pulsar discovery and basic properties

Pulsars were serendipitously discovered in 1967 during a low frequency survey (81 MHz) of extra-galactic radio sources. Over the years as technology and computation power became more advanced, optimal match filtering techniques allowed astronomers to obtain unaltered origin signals. Surrounding terrestrial equipment such as radars, electric cattle fence, transmission lines etc. showed up as pulses to the astronomers. Another point is that pulses from astronomical distances imply that source must be having very high brightness temperature around 10^{28} K which is far greater than 10^{12} K (limiting brightness temperature of any incoherent emission process such as electron Synchrotron radiation). Nevertheless, a graduate student from Cambridge University, Jocelyn Bell, noticed pulses in her scintillation survey data because they appeared by about 4 minutes every solar day and exactly once per sidereal day. Thus it was concluded that signal was from outside solar system.

The electromagnetic waves emitted by pulsars is generated at the cost of its rotational energy. Considering these pulsars as rotating magnetic dipoles which are known to lose energy in the form of radiation. Because of losing energy via radiation they slow down and this is called 'Spin-down'. By equating power of magnetic dipole radiation with loss in rotational kinetic energy, we get

$$\dot{E} = I\Omega\dot{\Omega} = 2/3 * \frac{m_B^2 * \Omega^4 * \sin^2\alpha}{c^3}$$

where \dot{E} is the loss in rotational kinetic energy, Ω is angular velocity, $\dot{\Omega}$ represents angular acceleration, α represents the angle between magnetic axis and rotation axis, and c represents speed of light.

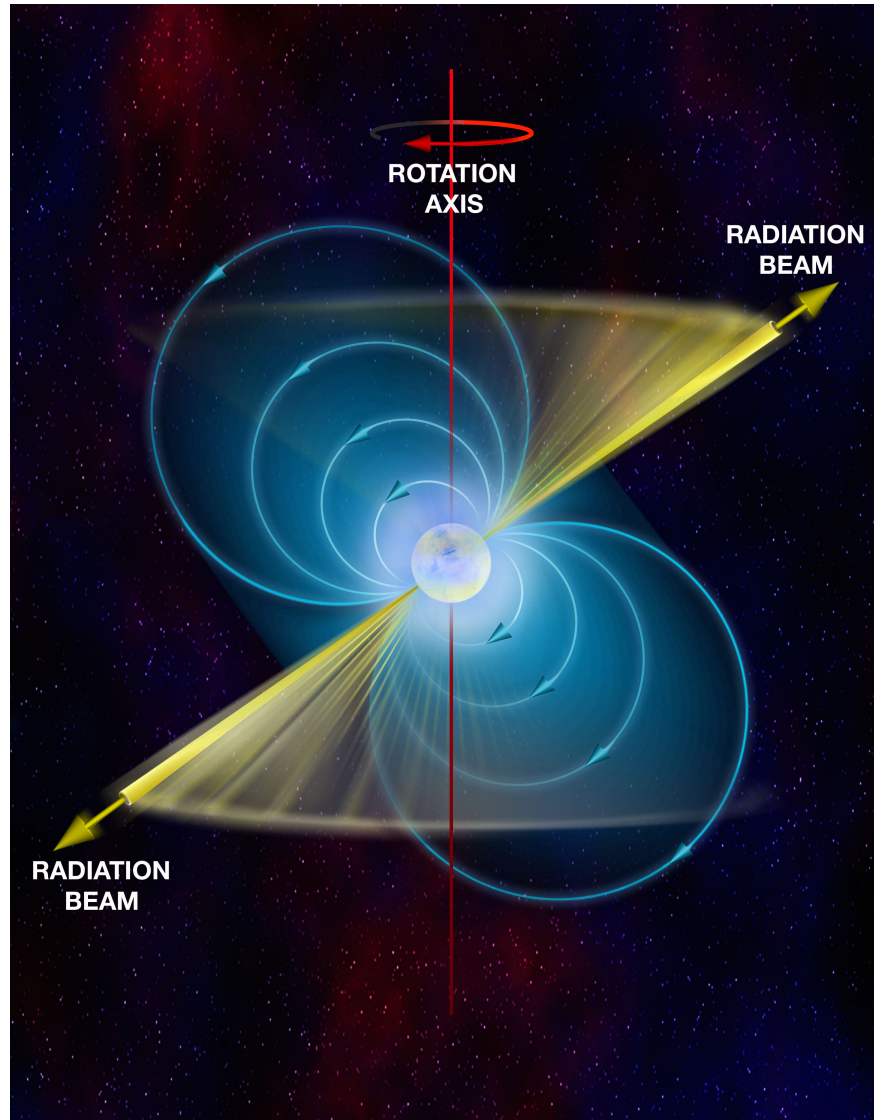


Figure 1.1: Model of rotating neutron star [9].

By proper arrangement of terms, we obtain an expression for spin evolution with time:

$$\dot{\Omega} \propto -\Omega^3 \sim \Omega^n$$

where n is the braking index. For a magnetic dipole radiation, $n = 3$. Hence, the spin frequency evolution of the pulsar is highly dependent on the value of spin frequency. The spin frequency evolution also predicts the evolution of spin period. Under certain assumptions, we can also predict the ‘characteristic age’ of pulsar (characteristic age is the age of pulsar calculated

assuming that spin evolution was constant with time).

$$Age = \frac{1}{n-1} \frac{P}{\dot{P}}$$

As spin-down is related to magnetic field (B), it can be predicted from the observations of the period (P) and period derivative (\dot{P}) in the following manner [10].

$$B = \frac{3c^3 I}{8\pi^2 R^6 \sin^2 \alpha} P \dot{P}$$

where B represents dipolar magnetic field at surface of neutron star, R is radius of the pulsar, and I is moment of inertia of the pulsar.

1.1.2 Observing pulsars

Pulsars emit mostly in low frequency radio regime around 400 MHz. These radio waves, on their way through the interstellar medium to earth, suffer some propagation effects. One of the major effects of propagation is: Dispersion.

Dispersion involves radio waves interacting with the electrons in interstellar medium (ISM), where low frequency waves are delayed and high frequency waves arrive earlier. This effect is illustrated in Figure 1.2.

The pulses at different frequencies are delayed depending on the plasma frequency of the electrons in ISM, which is directly proportional to square root of ISM electron density. This effect smears out the original folded pulse and hence this dispersion effect needs to be compensated for to get the original unaltered signal. This process is called "de-dispersion". In this process while recording the pulse profile, the pulses at different frequencies are corrected for the dispersion delay before summing up the signals from all the frequency channels. If the pulse profiles are not de-dispersed, we might obtain blurred and smeared pulse, and in certain cases even no pulse is detected. Mathematically, the 'time delay' in milliseconds due to dispersion effects is given by :

$$delay = 4.15 \times 10^6 \times [\nu_{low}^{-2} - \nu_{high}^{-2}] \times DM$$

where constant DM represents dispersion measure in units of pc cm^{-3} , ν_{low} and ν_{high} represents high frequency and low frequency in MHz [10].

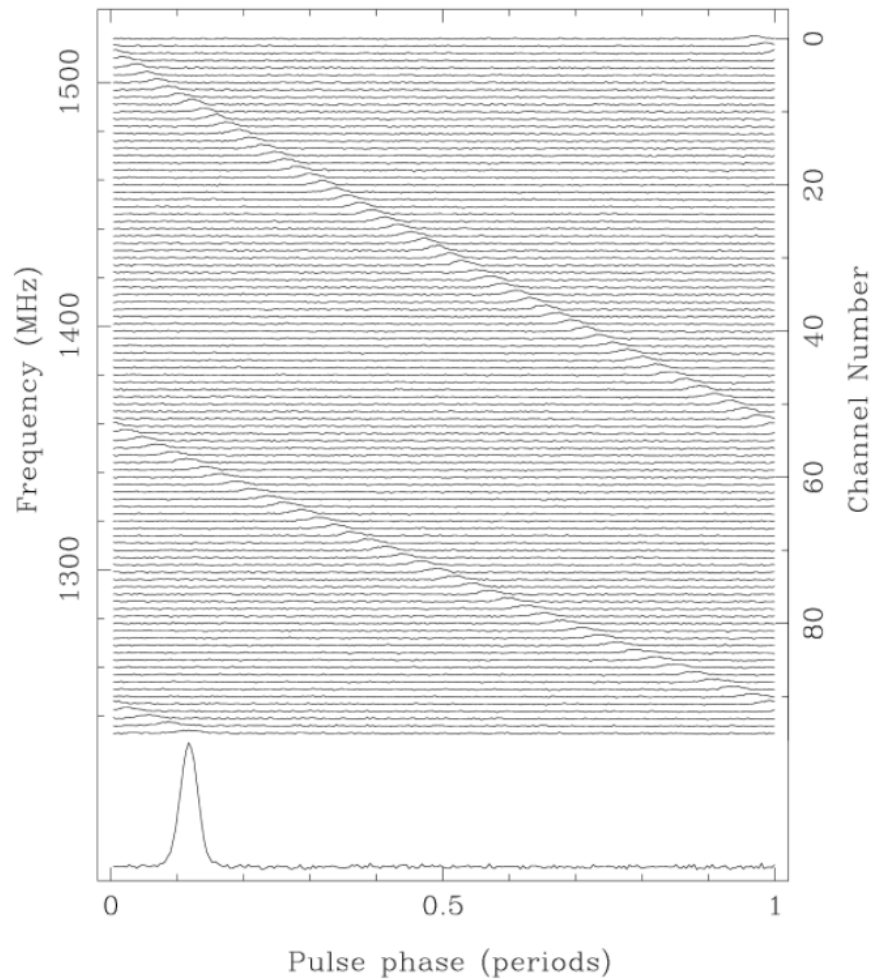


Figure 1.2: The dispersion effect to progressive delay in pulses at different frequencies [9].

1.1.3 Motivation

Pulsars are primary ways to detect neutron stars and offer a handy tool to probe various exotic physics associated with them.

- To probe physics of ultra-strong magnetic fields
- For studying the super-dense matter present at the neutron star core
- To probe Inter-stellar Medium
- To map precise timing evolution especially for gravitational wave detection purposes

- Gravitational physics in the strong field regime
- To study plasma physics in extreme conditions

1.1.4 Emission Mechanism

Classical rotation-powered pulsars having high magnetic fields ($10^{12} - 10^{13}$ G) can be represented as rotating magnetic dipoles. The pulsar surface magnetic field is non-aligned with the rotational axis resulting in an emission similar to a rotating magnetic dipole. There are open field lines near the magnetic pole which are the magnetic field lines that originate on neutron star and end up at infinity and there are closed field lines which originate and end on the neutron stars itself. The field lines co-rotate with the neutron star till the point where the rotational speed of the lines equals the speed of light. This point where the rotational speed of the field lines reach speed of light is given by the light cylinder radius. The movement of electrons along the curved field lines results in the emission of curvature radiation which is highly polarised in plane of curvature. Near the surface, a strong electrostatic field is formed which accelerates the particles in the pulsar magnetosphere to ultra-relativistic energies, that results in a highly coherent beamed radiation along magnetic axis. The actual emission scenario, however, is highly complex and is crucially governed by the emission region physics and various second-order effects.

1.1.5 Emission properties

The pulses that we receive on earth from pulsars is due to lighthouse effect of emission beam which sweeps our line of sight once per rotation due to the misalignment of the pulsar's rotation and magnetic axis. The integrated pulse profile can be obtained after summing several hundreds to thousands of pulsar rotations. These profile might change with epoch and they might have several components within the pulse (Figure 1.3) depending on emission mechanism and pulsars orientation with respect to the observer. These pulse profiles can also be highly frequency-dependent as guided by pulsar emission spectrum. Here we focus mainly on studying the features within the individual pulses [9], the motivation and detailed background of which will be discussed in the following sections.

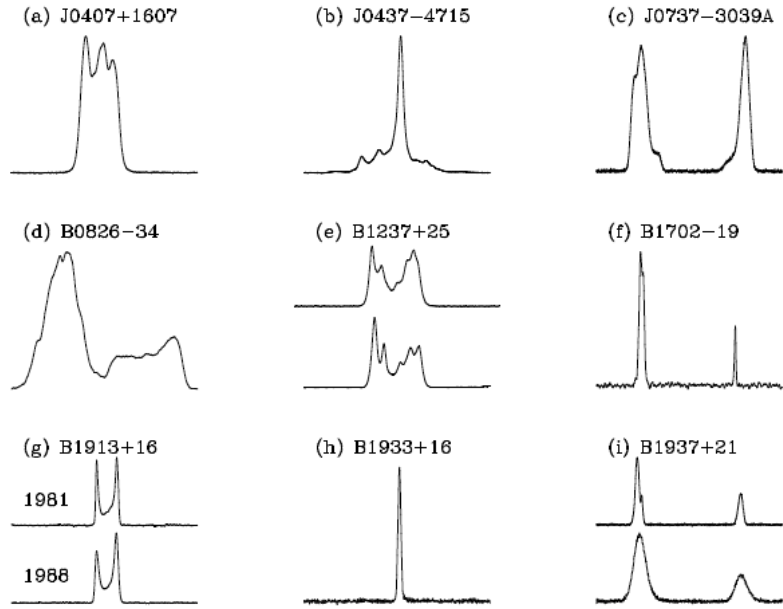


Figure 1.3: A sample of pulse profiles showcasing their varying nature and complex structure between different sources (a, b, c, d, f, h). The time evolution of the profile can also be observed often for the same pulsar as shown by e, g, and h [9].

Based on the observed pulse shapes, two phenomenological models were introduced to explain the observed pulse shapes and sub-pulse variations. Firstly, the ‘cone and core’ model which depicts the pulsar emission beam to be composed of a core surrounded by nested cones (left panel of Figure 1.4). The alternative is the ‘Patchy beam’ model which assumes the pulsar beam to comprise randomly distributed emitting regions (right panel of Figure 1.4). Further work is required to get a better understanding of shape and evolution of the emission beams. The pulse shape also depends on line of sight (LoS) of the observer with respect to the pulse beam.

1.1.6 Within these pulses

If the signal-to-noise ratio of the pulse signal is sufficient, we can obtain microstructures of each individual pulses. On investigating the individual pulses - single pulses - various features like nulling, sub-pulse drifting amplitude modulation can be observed each of which reveal information about the pulsar emission intricacies.

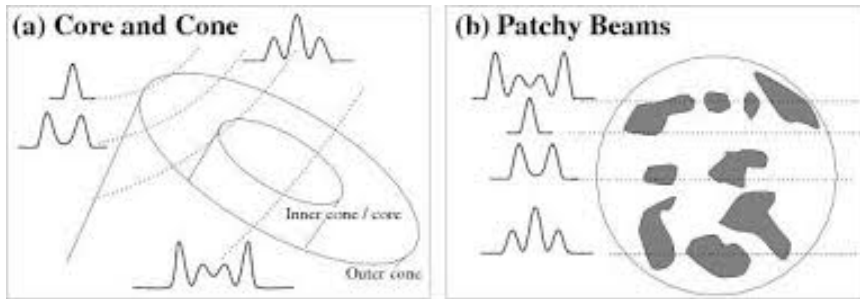


Figure 1.4: Emission models

1.1.6.1 Nulling

[16] first noticed the ‘nulling’ behaviour in pulsars. Nulling is the sudden absence of pulse in the observed pulse train from a pulsar. This nulling behaviour varies from pulsar to pulsar. [18] presented a correlation between nulling and age of pulsars. [17] later found some evidence showing inverse correlation between nulling fraction and pulse period. These evidences indirectly showed the weakening of emission process as the pulsar reaches the end of its active lifetime as pulsar.

1.1.6.2 Drifting subpulses

Sub-pulses are the pulses in a pulse train which on averaging produce the pulse profile. In some cases it was seen that these sub-pulses do not appear at the same phase over time i.e., these sub-pulses tend to drift. An explanation of this phenomenon was given by [19] where they estimated that sub-pulses are produced due to a rotating carousel of sub-beams (‘sparks’) with the hollow cone emission meet our line of sight. However, drift characteristics and its relation with the pulsar properties are not completely understood till date.

1.1.6.3 Periodic Amplitude Modulations

The presence of additional periodic behaviors were seen in fluctuation spectra which include periodic nulling and periodic amplitude modulation [3, 15, 20, 32]. Certain pulsars with low frequency emission show low frequency modulation in intensity of the pulses where core component also participates [25]. This behavior is known as periodic amplitude modulation. Periodic

features in fluctuation spectra can be identified as periodic modulation. Periodic amplitude modulation is seen in core as well as cone components [24].

The mechanism behind periodic modulations is still unknown, but is proposed to be distinctly different from subpulse drifting. These periodic amplitude modulations cannot be explained by PSG (Partial screen gap) model [35, 36], which explains the subpulse drifting phenomena. Such phenomenon is hypothesized to originate from temporal variations in the charge distribution or plasma flow in the pulsar magnetosphere. By recent studies it appears that, periodic amplitude modulation is also seen in interpulses observed from certain pulsars [3], implying modulation at both poles. The main pulse and interpulse seemed to show phase-lock between their modulation patterns and correlated behavior between sections of main pulse and interpulse, which suggests that there might be information transfer globally across the whole magnetosphere. Till now such periodic amplitude modulation is observed in about 29 pulsars and is observed to show wide time-variation and frequency dependence, that cannot yet be precisely modelled [20]. Further temporal and multi-frequency observations and modelling need to be carried to precisely infer the origin of periodic amplitude modulation. In our research, we carried out the low frequency study of these phenomena if they are present in the PSR J1825–0935 . No study of these phenomena at this low frequency from this pulsar was done earlier owing to lack of sensitivity, time resolution at these frequencies. But presently, with new highly sensitive current and upcoming telescopes, such as MWA (Murchison Widefield Array) - an SKA (Square Kilometer Array) precursor, this phenomenon can be studied at low frequencies at high sensitivity.

Next we discuss the distinction between various periodic modulations. Correlation of spin-down luminosity with drifting and non-drifting sub-pulses was observed by [20]. Among the 57 pulsars showing observed periodic features in sub-pulses, pulsars with $\dot{E} < 2 \times 10^{32} \text{ erg s}^{-1}$ showed sub pulse drifting and pulsars with $\dot{E} > 2 \times 10^{32} \text{ erg s}^{-1}$ showed non-drifting amplitude modulation [20]. Whereas the correlation between variation in spin-down rate and amplitude variation ratio was observed to be maintained over different epochs of time i.e., over a long timescale ($\sim 10 \text{ yr}$) [1, 21].

Detailed classification of sub-pulse drifting was carried out by [15]. Equivalent study on other periodic modulation process was done by [3]. Various characteristics of drifting sub pulses and periodic amplitude modulation are presented and compared in Figure 1.5.

	Subpulse Drifting	Periodic Modulations
Profile Component	(i) Only seen in conal components. (ii) Different phase variations for different components.	(i) Simultaneously seen in central core and cones. (ii) longitude stationary, similar across all components.
Spindown Energy	(i) Seen in pulsars with $\dot{E} < 5 \times 10^{32} \text{ erg s}^{-1}$. (ii) P_3 weakly anti-correlated with \dot{E} .	(i) Seen in pulsars with wide \dot{E} distribution. (ii) $P_M \sim 10\text{-}200P$, no dependence of P_M on \dot{E} .
Origin	(i) Localised in Inner Acceleration Region. (ii) Associated with sparking process of plasma generation.	(i) Seen in both poles of pulsars with interpulse emission. (ii) Largescale variations affecting pulsar magnetosphere.

Figure 1.5: Comparison of periodic characteristics of radio pulsars [3].

The dependence of modulation periodicity (P_M) on radiated power (\dot{E}) was estimated to be as shown in Figure 1.6 [3]. The Figure 1.6 consists

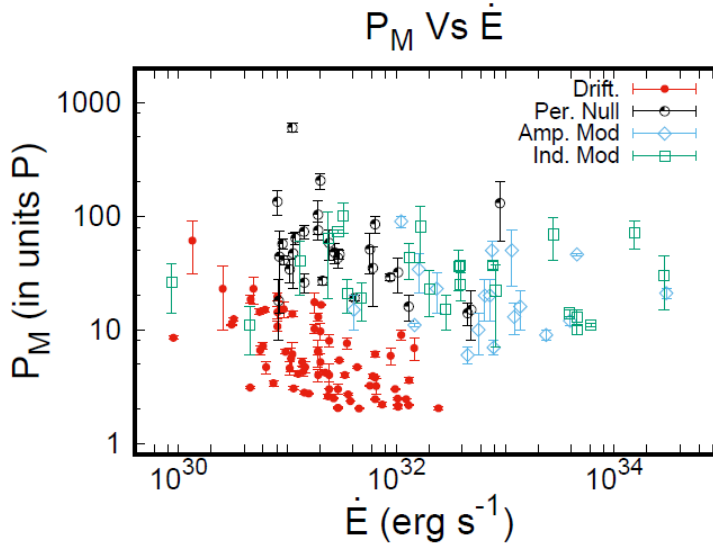


Figure 1.6: Distribution of modulation periodicity with spin-down energy \dot{E} for various pulsars [3].

of three categories of pulsars exhibiting different periodic modulations. Pulsars showing periodic nulling are represented by ‘black open circles’, pulsars showing amplitude modulations are represented by ‘blue rhombus’ and those displaying intermediate modulations (requiring high sensitivity)

are represented by ‘green square’ and the fourth category - drifting sub-pulses are represented by ‘red filled circles’. Distribution of these categories in the plot gives the distinction between drifting sub-pulses and the other periodic modulations with the former three categories pulsars being superimposed in terms of distribution.

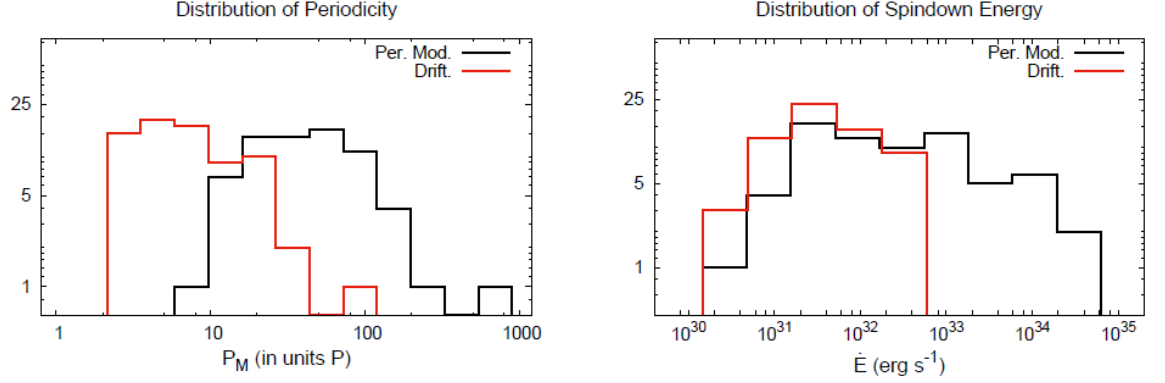


Figure 1.7: The left panel shows distribution of modulation periodicity in units of the pulsar period P and right panel distribution of spin-down energy for drifting and other sub-pulse modulations [3].

The differences between the distribution of the physical parameters for the sub-pulse drifting and the other periodic modulations are clearly demonstrated by the plots in Figure 1.7. The periodic modulations have periodicities ranging from $10 - 200P$ (where P is the period of pulsar) with peak around $50P$, whereas drifting ones showed periodicity of $20P$, with distribution peaking around $5P$. The drifting sub-pulses in \dot{E} distribution reaches maximum value around $3 \times 10^{31} \text{ erg s}^{-1}$, with peak value around $2 \times 10^{32} \text{ erg s}^{-1}$, whereas periodic modulations seem to show wider distribution of \dot{E} , ranging from 10^{31} to $10^{34} \text{ erg s}^{-1}$.

Chapter 2

Murchison Widefield Array (MWA)



Figure 2.1: Array of dipole antennas- MWA [8].

The Murchison Widefield Array (MWA) is an international low frequency telescope located at mid-west Australia. It is about 200 km from the coastline, with extremely low levels of radio frequency interference (RFI). This array consists of 4096 dipole antennas (Figure 2.1) to facilitate the detection in low frequency regime of 70-300 MHz. This telescope array has been identified as one of the SKA (Square Kilometre Array) precursors. This array has got

no moving parts and for pointing any location in sky electronic manipulation of dipole signals is performed. These antennas are arranged in 256 regular grids covering several kilometers. The data obtained from these antennas is correlated onsite before being sent to a long term storage facility called 'Pawsey Supercomputing centre'. The pulsar data is captured in the VCS (Voltage Capture System) mode, which is a functionality to capture raw voltages streaming into the correlator, from all 128 tiles, at $100 \mu\text{s}$, 10 kHz resolutions, over a bandwidth of 30.72 MHz. This gives an aggregate data rate of roughly 28 TB per hour. Its backend is an online platform - MWA node of all sky virtual observatory (MWA-ASVO) [8].

MWA was initially formulated as 512 tiles instrument to be built in several stages. The first stage was completed in late 2012, and it was commissioned in mid 2013, which consisted of only 128 phased tiles where each tile consisted of 16 crossed dipoles arranged in a 4×4 square. The commencement of phase 2 was in 2017 and commissioned in August 2018. Enhancement of the instrument was performed in phase 2 where sensitivity of the instrument was raised by a factor 10. Further detail of MWA is summarized in Figure 2.2.

MWA majorly contributes in four science themes namely study of Galactic and extra-galactic processes, detection of fluctuations in brightness of hydrogen 21 cm line from the epoch of reionisation (EoR), study of time domain astrophysics through the radio sky (transients) and study of solar heliosphere and Ionosphere by imaging the propagation effects on background radio sources.

2.1 Role of MWA in pulsars study

As MWA is a low frequency observatory, we can take advantage of the steep spectrum of pulsars to obtain data with enhanced sensitivity. Its high sensitivity enables us to study especially various single pulse studies such as pulse nulling, sub-pulse drifting, mode switching which are more prominent at low frequencies. None of the available telescopes observe pulsars at such low frequencies with the required sensitivity which will let us get better understanding of mysterious emission mechanisms in pulsars. This

Property	Description
Frequency Range	70-300 MHz
Number of receptors	2048 dual-polarization dipoles
Number of antenna tiles	128
Number of baselines	8128
Collecting area	Approx. 2000 sq. meters
Field of view	Approx. 15-50 deg. (200-2500 sq. deg.)
Instantaneous bandwidth	30.72 MHz
Spectral resolution	20 kHz
Temporal resolution	0.5 seconds
Polarization	Full Stokes (I,Q,U,V)
Array configuration	<ul style="list-style-type: none"> • Phase I <ul style="list-style-type: none"> ◦ 50 antenna tiles within 100 meters of array centre ◦ 62 antenna tiles between 100 and 750 meters ◦ 16 antenna tiles at 1500 meters • Phase IIa (Hex/Compact) <ul style="list-style-type: none"> ◦ 128 antenna tiles within 300m • Phase IIb (Long Baselines/Extended) <ul style="list-style-type: none"> ◦ 42 antenna tiles within 500 meters ◦ 32 antenna tiles between 500 and 1000 meters ◦ 54 antenna tiles over 2500m meters

Figure 2.2: MWA configuration [8]

sensitivity also facilitates the study of pulsars in globular clusters and also let us observe the giant pulses (which was rarely observed due to limitations to pulsar observing and data processing techniques).

Chapter 3

Source and observation

3.1 Source

The selected source for this project using MWA is the pulsar PSR J1825-0935. It is a young pulsar with age of 233,000 years with a rotation period (P) of 769 ms, \dot{P} of $5.233 \times 10^{-14} \text{ s s}^{-1}$, DM (dispersion measure) of 19.38 pc/cm^3 , magnetic field of $6.42 \times 10^{12} \text{ G}$ [6].

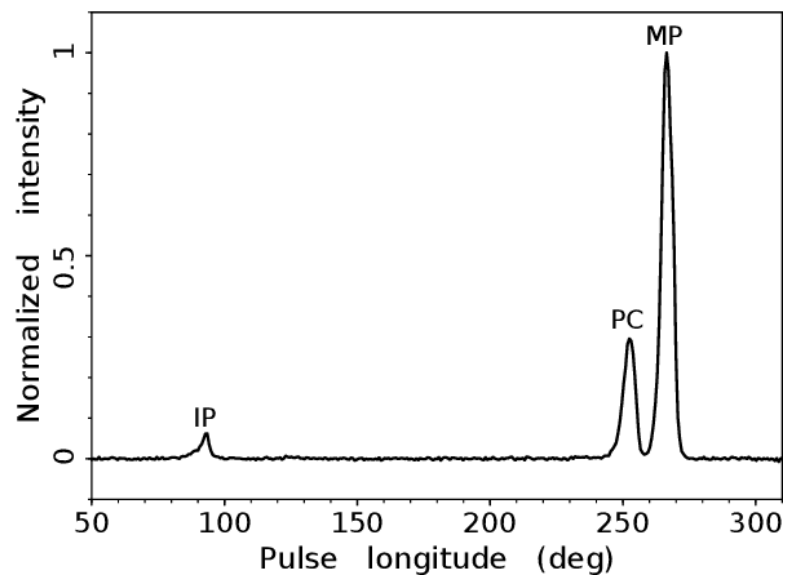


Figure 3.1: Mean pulse profile of PSR J1825-0935 [1].

The mean pulse profile of this pulsar has been observed to exhibit 3 components namely: main pulse (MP), interpulse (IP) and a precursor (PC)

as shown in Figure 3.1 [1]. The PC precedes MP by about 14.5° of pulse phase and the IP leads PC by about 159° . The pulsar exhibits three interesting features simultaneously: mode changing, PC and IP anti-correlation and periodic amplitude modulation. Mode changing refers to pulsar switching between two or more emission states in abrupt fashion. This pulsar has two modes namely: radio bright mode (B-mode) and radio quiet mode (Q-mode). Presence of strong PC component is considered as B-mode and strong IP component is considered as Q-mode (as IP and PC are anti-correlated) [1]. [27] reported about mode changing for every 5 minutes. While with 8 hours observation, [28] reported mode changing for about 7.6 minutes. From longer multi-frequency observations made by three different radio telescopes, [29] reported mode changing for every 3.5 minutes. [30] reported the correlation between modes and spin down rate changes in PSR J1825–0935.

[28] found presence of sub pulse drifting and periodic amplitude modulation in both modes of PSR J1825–0935, which was the study done at 325 MHz. [1] reported the presence of periodic amplitude modulation and absence of sub-pulse drifting using Parkes 64-m radio telescope at 1.4 GHz. The period of the periodic amplitude modulation was found to be similar at both frequencies ($43P$ in radio quiet mode), where P is the rotation period of the pulsar.

In this project, we focus on the periodic amplitude modulation aspect at low frequency i.e., 184.96 MHz. This was the first time this source was observed at such a low frequency with this high sensitivity, thereby providing a golden opportunity to perform single-pulse studies of PSR J1825–0935 at low frequencies. The data used for this work was taken on 9th June, 2020 and 19th June, 2020 using MWA under a proposal (PI: Parul Janagal) to observe single pulse behavior from sample of pulsars exhibiting interesting single pulse features. The details of the observation are as follows:

Project ID	G0071
Observation date	09/06/2020
Observation start time	17:27:27
Observation duration	2693.208 s
RA (deg)	276.37745833333
DEC (deg)	-9.589222222
Azimuth (deg)	358.5844
Zenith (deg)	17.13143
Central freq (MHz)	184.96
Low channel (MHz)	169.604995
High channel (MHz)	200.315002
Total Bandwidth (MHz)	30.7200671
Number of channels	3072

Table 3.1: Details of the MWA observation of PSR J1825–0935 used for single-pulse analysis(Epoch I).

Project ID	G0071
Observation date	19/06/2020
Observation start time	16:30:00
Observation duration	2693.208 s
RA (deg)	276.37745833333
DEC (deg)	-9.589222222
Azimuth (deg)	13.60049
Zenith (deg)	17.56601
Central freq (MHz)	184.96
Low channel (MHz)	169.604995
High channel (MHz)	200.315002
Total Bandwidth (MHz)	30.7200671
Number of channels	3072

Table 3.2: Details of the MWA observation of PSR J1825–0935 used for single-pulse analysis(Epoch II).

Chapter 4

Methodology and Results

Since MWA is a set of dipole antennas, the whole array is essentially looking at the whole sky at any given instance. The calibration solutions are calculated after the observation and the data is calibrated and beamformed, using a set of robust pipelines. The beamformed data is then converted to the PSRFITS format, which can also be converted to the filterbank format. These filterbank files contains all the information across phases and channels. For studying any pulsar, in the first step, we need to get its integrated pulse profile. Getting the integrated pulse profile involves taking the filterbank data, RFI (radio-frequency interference) removal, de-dispersing, Fourier transforming, binary delay correction, candidate selection, and pulse folding as depicted in Figure 4.1. Multiple software packages were developed to automate this process to obtain the best signal-to-noise ratio and to cater the various scientific needs.

4.1 PRESTO

One of such software packages is PRESTO developed by Scott Ransom [11]. Here we observed the pulsar PSR J1825–0935 in the low frequency regime in 185 MHz band using Murchison Widefield Array and obtained the corresponding data as described in the previous section. We worked with 2600s of the MWA data of this pulsar and performed the generation of the pulse profile using PRESTO. Using PRESTO the profile from the

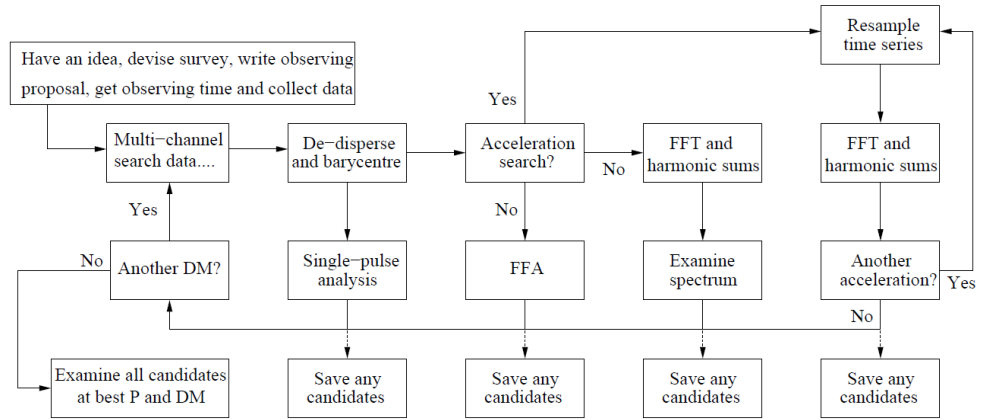


Figure 4.1: Flow chart of data flow for obtaining pulsar candidates [9].

entire data could not be generated possibly due to computational limitations. We generated the pulse profile from 200 s chunks of the observations time. One such pulse profile of PSR J1825–0935 is depicted in Figure 4.2. We obtained the dispersion measure and pulse period values as 19.38 pc/cm^3 and 0.769 seconds respectively which were consistent with the values in the literature for this pulsar. Hints of the interpulse could be observed in the average profile plot (top-left corner), however the strength was too weak to comment any further on the presence of an interpulse at this stage.

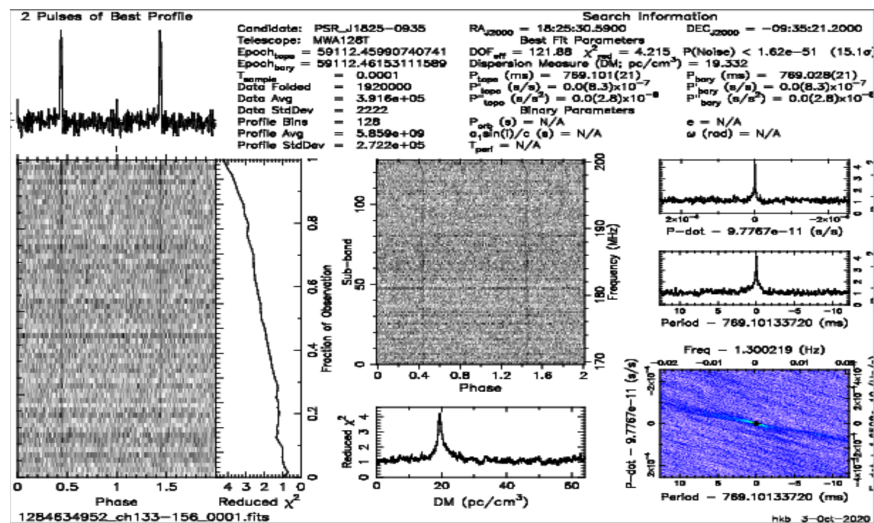


Figure 4.2: Folded pulse profile plot of PSR J1825–0935 for 200 s observation time generated using PRESTO

4.2 DSPSR

For more detailed and advanced (single-pulse) analysis, the data reduction was then performed using the DSPSR package [12] to de-disperse and produce single-pulse integrations which were recorded using PSRFITS data format [13] with 512 phase bins per rotation period. The pulsar's ephemeris was taken from ATNF Pulsar Catalogue v 1.64 [6] and we obtained different parameters such as various polarisation (I, Q, U, V) frequency, time etc i.e, a multidimensional data as shown in the Figure 4.3 which was saved in the output files for further analysis.

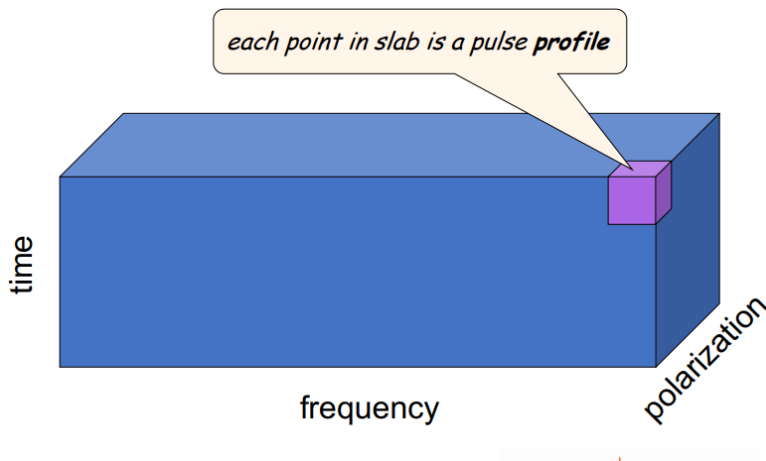


Figure 4.3: Format of data in DSPSR [14]

We further reduce this data into a three-dimensional format which contains information about the profile of each single pulse (pulse number, intensity, phase) by compressing the data over the polarization and the frequency axes and generated the single-pulse profiles. They were further converted into the ASCII format.

Using the data obtained using the aforementioned procedure, we carried out an investigation of the single pulse profiles especially with aim of studying amplitude modulation of the single pulse train.

For this goal, the ASCII data was handled using Python v2.7 and algorithms were developed to obtain the single-pulse parameters like pulse energy and the phase-dependent pulse modulation index. For a consistency check, we first created the averaged pulse profile combining the data from

the entire 3500 s and 6500 s exposure time for 2 epochs respectively.

4.3 Binning

Binning is a way to handle noisy data, or it is used to smoothen data. This method consults the neighborhood of values and performs local smoothing. There are three ways to approach binning/smoothing:

1. Smoothing by bin means
2. Smoothing by bin median value
3. Smoothing by bin boundary

Here we adopt binning by means method to reduce noise content in our data. Care needs to be taken while binning data, as over- binning might remove or reduce even the signal content and under-binning might contain relatively fair amount of noise in data. Here in our work, based on the length of time series, we calculated and plotted pulse energy vs pulse number graphs binning at different numbers as mentioned in pulse energy section of report.

4.4 Pulse profile

Pulse profile basically gives the information about the pulsars in the form of EM wave emission. Integrated pulse profile is obtained when the whole observed pulse profile is folded upon itself at the particular period of the pulsar. This period can be obtained by the calculating the Fourier transform of the observed time series after various time corrections. The integrated pulse profiles of the PSR J1825-0935 was obtained for 2 epochs with pulse numbers 3500 and 6500 respectively. They are shown in Figure 4.4 and Figure 4.5. A slight variation in the profile morphology can be observed between the averaged pulse profile of epoch I to epoch II.

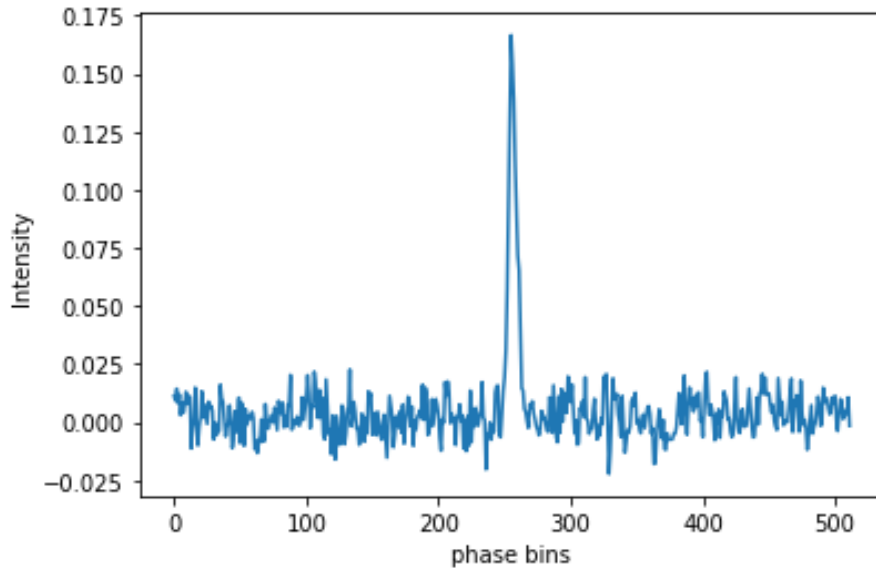


Figure 4.4: Averaged pulse profile from PSR J1825–0935 computed over the entire 3500 s (epoch I). The strong main pulse can be very clearly seen, however no strong evidence of any interpulse is present.

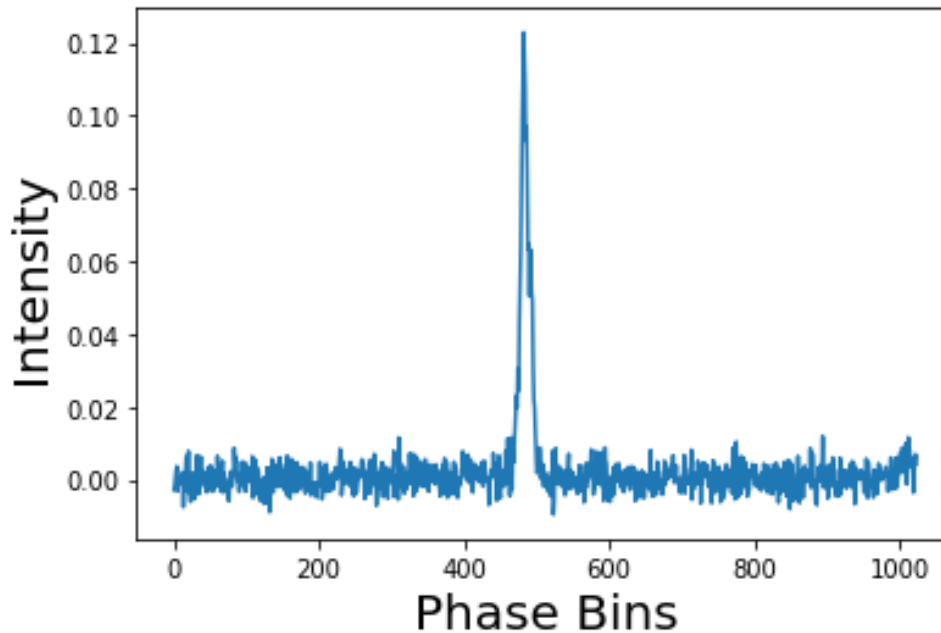


Figure 4.5: Averaged pulse profile from PSR J1825–0935 computed over the entire 6500 s (epoch II). The strong main pulse can be very clearly seen, however a very weak indication of an interpulse can be observed.

4.5 Pulse stack

Single pulse stack is a 2-D representation of intensity across the phase bins and the pulse numbers. It gives an idea about how the signal strength is varying with time (increasing pulse number) in each phase bin. Here on Y-axis we have pulse number and on X-axis we have phase bins. The colour in the plots represents the strength of signal where yellow colour represents higher strength and blue colour represents lower strength. However, the single-pulse signal we obtained is of low strength. To further assess its properties in 2-D plot, we averaged the pulse strength for every 10 pulse numbers, to increase the signal-to-noise ratio of the pulse signal. The resultant pulse stack plots are shown in Figure 4.6 and Figure 4.7.

A clear variation in strength of the signal can be observed in the 2-D pulse stacks. However, the variation in the two epochs is different. This might give us a clue about amplitude modulation, a phenomenon usually

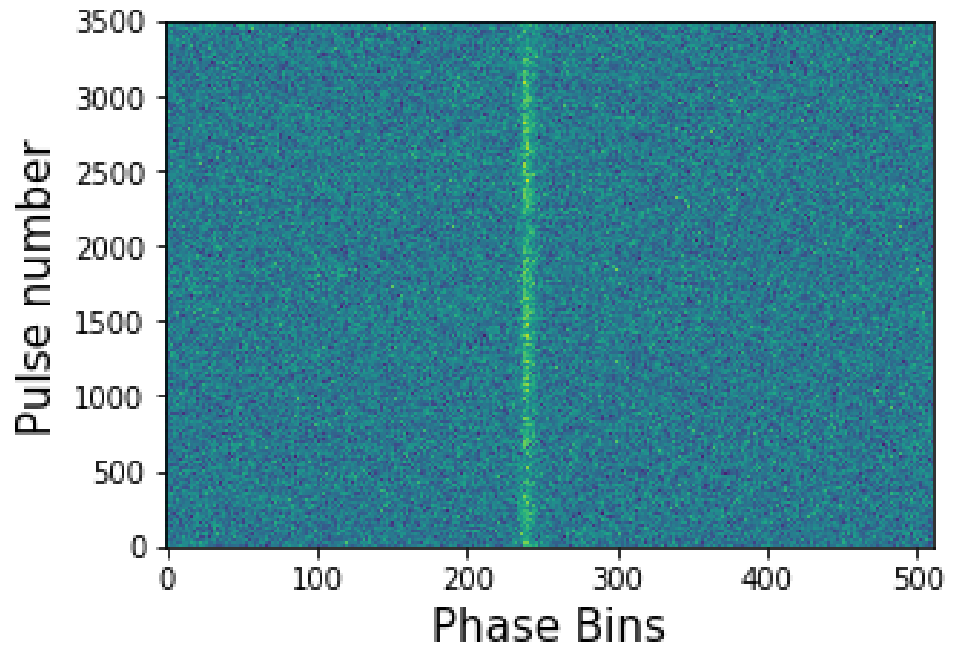


Figure 4.6: 10 binned pulse stack from PSR J1825–0935 computed over the entire 3500 s in epoch I. Variation in the strength of the pulse signal can be clearly seen in this plot.

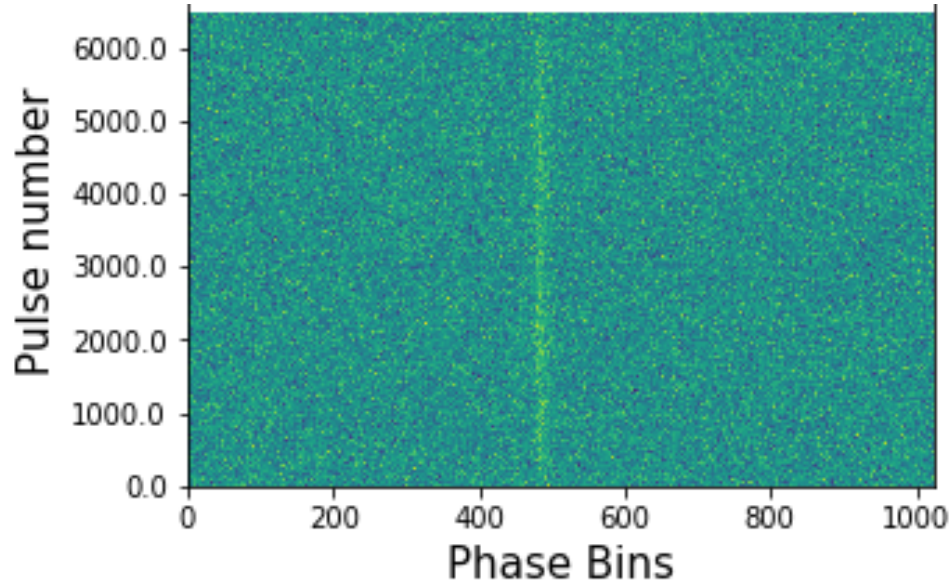


Figure 4.7: 10 binned pulse stack from PSR J1825–0935 computed over the entire 6500 s in epoch II. Variation in the strength of the pulse signal can be clearly seen in this plot.

seen in pulsars. So this observed feature can be used to study amplitude modulation property in this pulsar.

4.6 Modulation Index

To quantify the intensity variability or amplitude modulation across the pulse train and to examine its phase dependence, we computed the modulation index for the pulse. In general, the modulation index of a statistic ‘X’ is the square root of variance divided by mean value of statistic ‘X’. In this case, we take intensity, which is a function of phase, to be the statistic. Hence, the phase resolved modulation index $m(\phi)$ is given as

$$m(\phi) = \frac{\sqrt{\langle I^2(\phi) \rangle - \langle I(\phi) \rangle^2}}{\langle I(\phi) \rangle}$$

It is represented as the ratio of the square root of variance of intensity to the average value of intensity (I), where intensity is a function of phase (ϕ). If there is no variation in statistic, we get modulation index $m(\phi)$ to be ‘zero’ and it is ‘non-zero’ in the case any variation exists. The numerator of the above expression in this case is defined as the standard deviation.

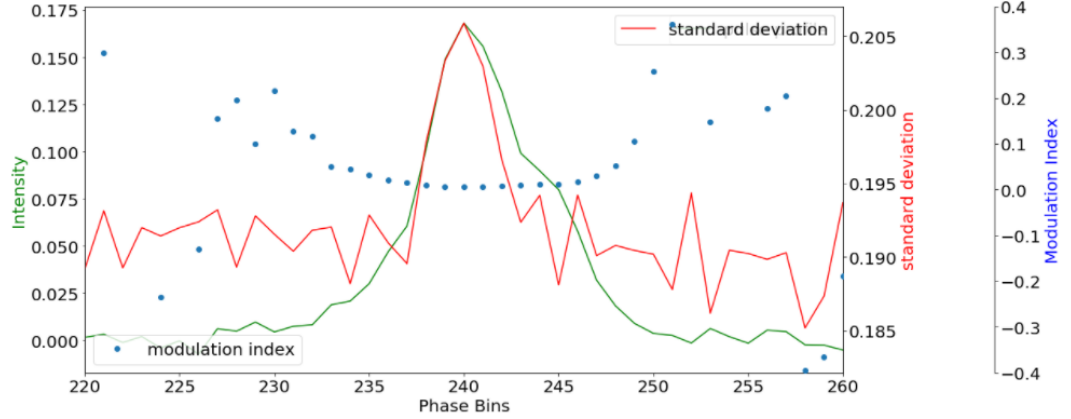


Figure 4.8: Modulation Index of amplitude variation across the pulse profile of PSR J1825-0935 for epoch I. The green solid line shows the pulse intensity, the red solid line represents the standard deviation and the blue circles represents the modulation index.

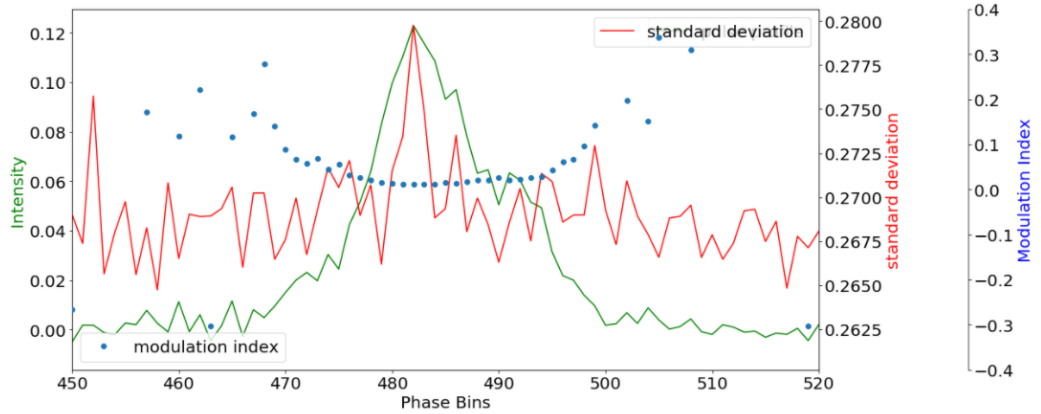


Figure 4.9: Modulation Index of amplitude variation across the pulse profile of PSR J1825-0935 for epoch II. The green solid line shows the pulse intensity, the red solid line represents the standard deviation and the blue circles represents the modulation index.

Figure 4.8 and Figure 4.9 shows the phase-dependent modulation index computed from the entire pulse train plotted across the phase the bins for epoch I and epoch II respectively. It can be seen that we find different level of amplitude variation at different phases within the pulse, i.e, the trailing part shows more variation in intensity with pulse number when compared to the leading part of the pulse and variation in central phase was found to be

minimum. But in the second epoch, quite opposite behavior was found, i.e, the leading part of the main pulse showed more variation in intensity than the trailing part. It certainly shows that the emission mechanism involved might be transient and time-variable in nature, so PSR J1825–0935 showed a change in the modulation index from epoch I to epoch II.

4.6.1 LRFS

LRFS stands for longitude-resolved fluctuation spectrum which displays the presence of any periodic signal power as a function of frequency and pulse phase. Performing LRFS analysis on any pulsar data, gives us the presence of periodicities for each pulse longitude bin. For the two epochs, LRFS analysis was performed. The pulse stack is divided into 6 blocks of 512 successive pulses for epoch I and 12 blocks of 512 successive pulses for epoch II. Subsequently, LRFS was calculated by performing the discrete Fourier transform on these blocks for both the epochs and following results are exhibited in Figure 4.10 and Figure 4.11 for epoch I and epoch II respectively. In these figures, the 2-D greyscale plot displays the power as a function of the phase in X-axis and fluctuation frequency in Y-axis. The greyscale represents the fluctuation power, with white representing higher power. On the right panel the fluctuation power spectrum is shown where averaging along the phase axis was applied.

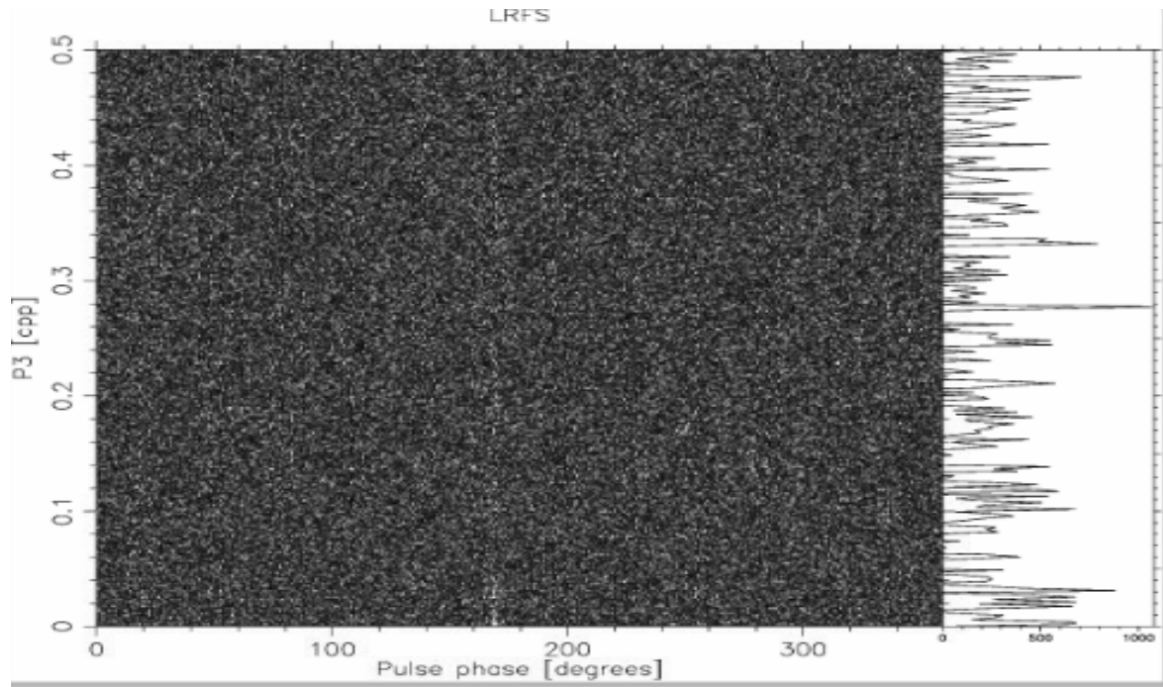


Figure 4.10: LRFS of PSR J1825–0935 for whole epoch I, taking blocks of 512 length FFT

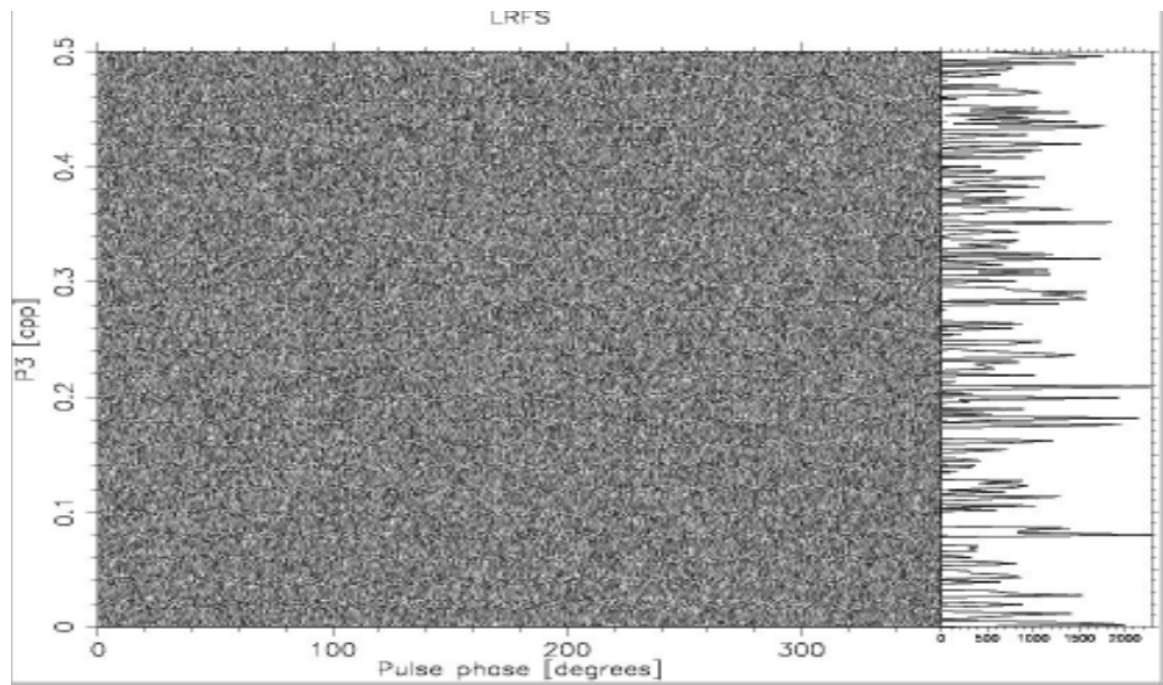


Figure 4.11: LRFS of PSR J1825–0935 for whole epoch II, taking blocks of 512 length FFT

However, both plots seem to show that signal strength is not enough to perform longitude resolved fluctuation spectrum analysis. Furthermore, it indicates that a fluctuation signal if present, has to be transient and non-stationary, otherwise such a signal would show up, albeit weakly, in this plot as it was generated adding data from all the pulses in the data for each epoch.

4.7 Pulse energy

To study the variations in the pulse emission strength observed in the single pulse stack plots, the pulse energy was plotted against pulse number for both epochs. Here pulse energy was defined as the area under the on-pulse region. Carrying out this exercise might help us understand what type of periodic modulations are seen i.e, nulling, amplitude modulation (both periodic and non-periodic ones). As amplitude modulation was seen in the pulse energy vs pulse number plot. We proceeded with binning by 10 pulse numbers for further studies to increase the signal-to-noise ratio of any possible signal present in the data. Figure 4.12 shows the variation of pulse energy between around -2 to 4 units with the pulse numbers (time) for epoch I. Figure 4.13 shows the variation of pulse energy from -5 to 5 units for epoch II. It can be observed that pulse energy variation in second epoch showed a relatively higher global variation behavior compared to the pulse energy variation in epoch I.

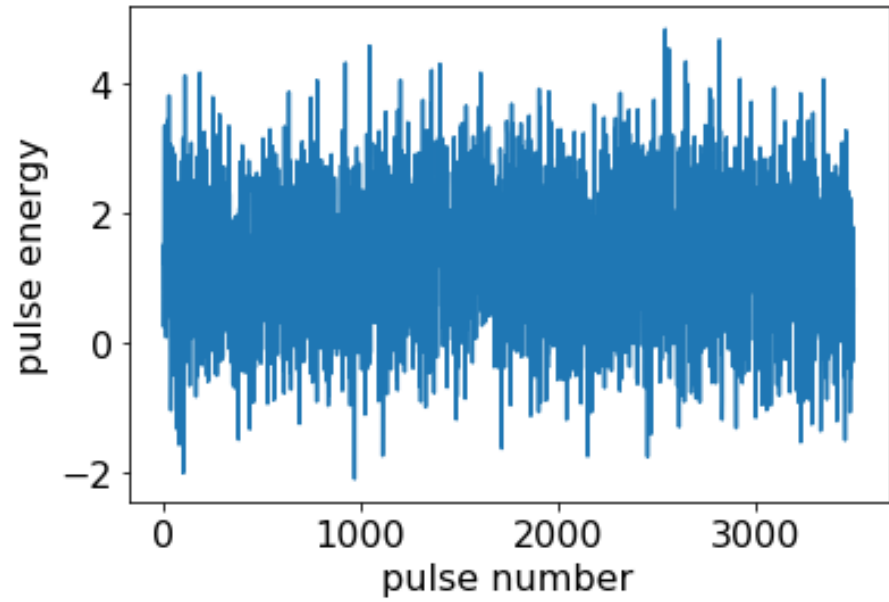


Figure 4.12: Pulse energy variation across whole time of observation of PSR J1825-0935 for epoch I

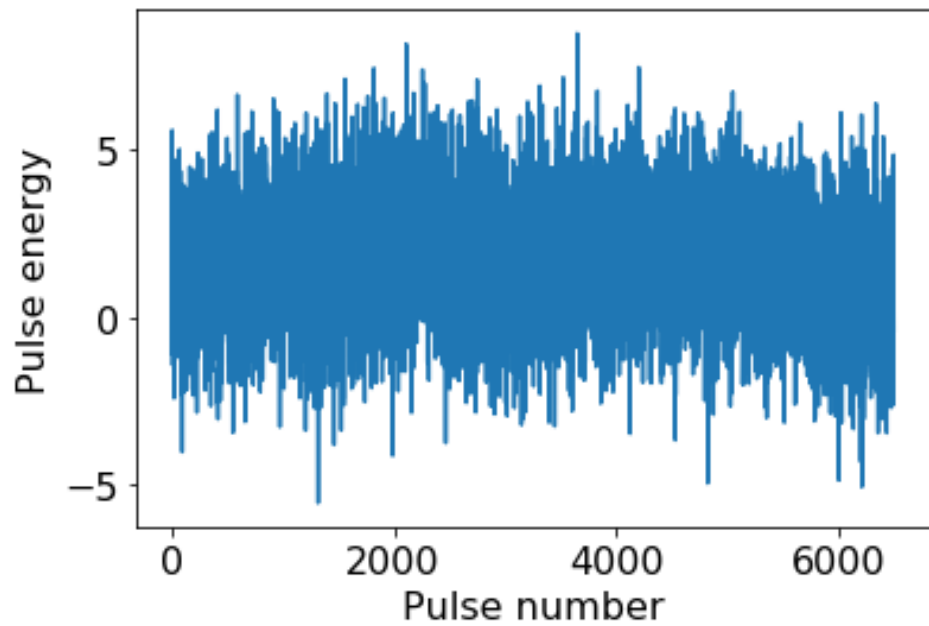


Figure 4.13: Pulse energy variation across whole time of observation of PSR J1825-0935 for epoch II

4.7.1 Pulse energy studies - epoch I

Figure 4.12 shows the observed variation in pulse energy. If any pattern is present in the variation of amplitude, and if it is a stationary time series, a simple Fourier transform could reveal the periodicity if it is present. But it can be seen Figure 4.12 represents a non-stationary time series, meaning the periodicity of any modulation seems variable. In such non-stationary time series, periodic nature can be revealed by obtaining sliding Fast Fourier Transform (FFT) of the respective non-stationary time series. The sliding FFT technique was applied to epoch I. The length of segment considered was 512 pulses and the length of sliding was 10 pulse numbers. The Nyquist frequency obtained was 0.63 Hz. The resultant dynamic power spectrum for epoch I that was obtained through this exercise is shown in Figure 4.14.

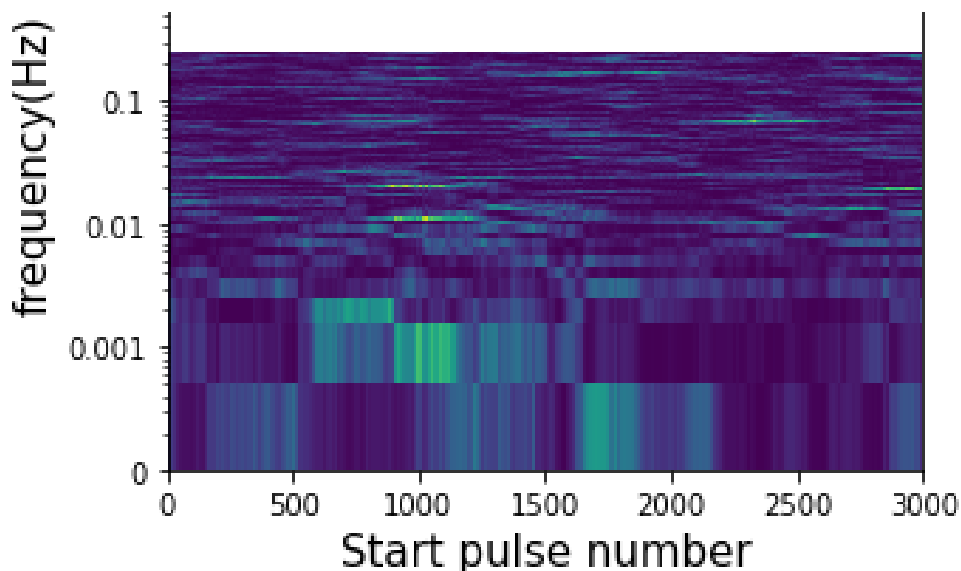


Figure 4.14: Sliding FFT method applied to the non-stationary pulse energy vs. pulse number series for epoch I.

In Figure 4.14, some yellow structures, representing higher signal strength or presence of modulations, can be observed in pulse number range 800-1400. The frequency corresponding to that modulation was observed to be around 0.011 Hz. To further verify this claim, a conventional Fourier transform was applied in the pulse number range 800-1400, and the resulting frequency was found to be 0.066 Hz. Figure 4.15 shows the power spectrum

corresponding to conventional Fourier transform in the pulse 800-1400. The slight mismatch between the two frequencies results in an uncertainty in the presence and period of the modulation.

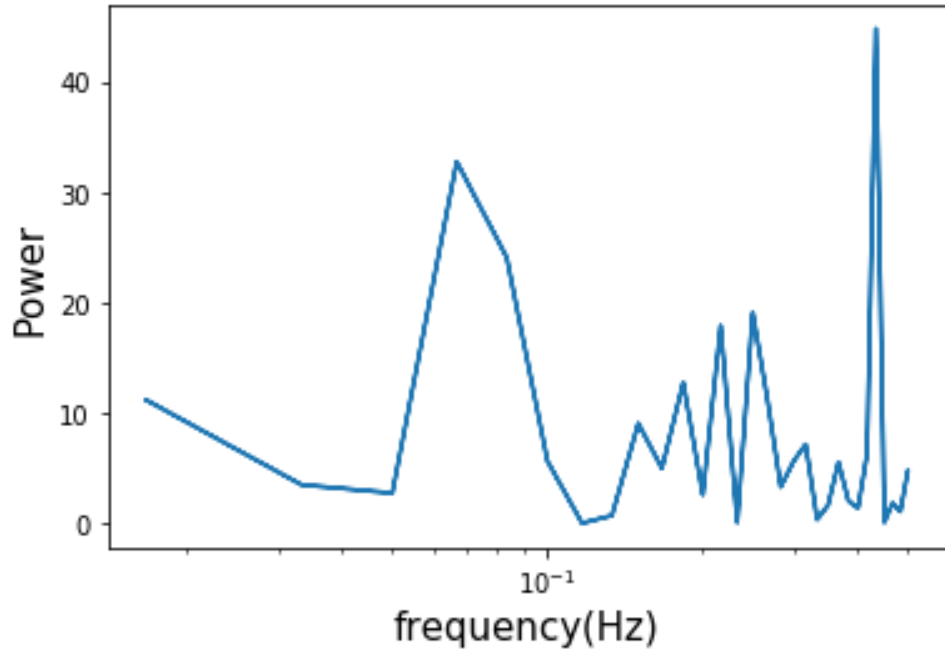


Figure 4.15: Power spectrum of the pulse energy region 800-1400

To further verify this and put stronger constraints on the modulation, we shifted the pulse region by ± 50 pulse numbers, and in these two adjacent pulse regions we again carried out the conventional FT. In the resultant power spectrum of these two regions, the frequency was observed to change abruptly to 0.43 Hz, whereas the presence of any real signal in these pulse numbers might have shown a gradual decrease or change in frequency. Since mismatch of frequency was observed, it was concluded that the presence of the modulation could not be confirmed with confidence and some significant noise contribution may be present.

4.7.2 Pulse energy studies - epoch II

As shown in Figure 4.13, a more pronounced global variation in pulse energy i.e., rapid and high change in pulse energy was observed for epoch II. To get a clear estimate of this global variation, the pulse energy plot

Figure 4.13 was binned by means for every 10 pulses, and it was fitted with a Gaussian filter with $\sigma = 4$. The result is shown in Figure 4.16.

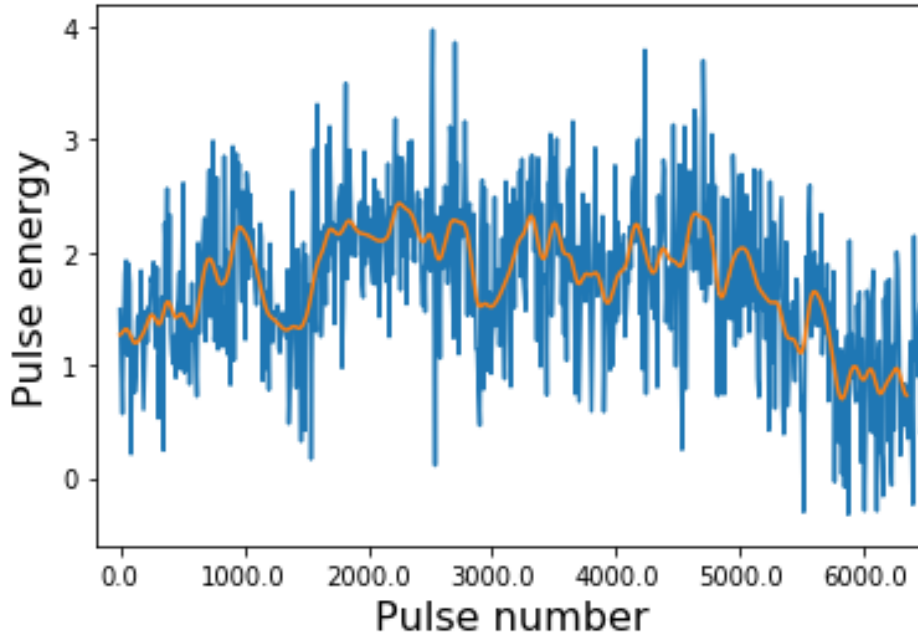


Figure 4.16: Pulse energy vs pulse number with 10 pulse averaging for epoch II. The orange solid line shows the Gaussian filter convolution of the underlying pulse energy plot.

The plot in Figure 4.17 can be seen consisting of various dips in pulse energy at certain pulse numbers. So whole plot was divided into several sections according to high and low pulse energy values as in Figure 4.17. The region where pulse energy was observed to dip considerably, was considered as weak state. Remaining cases were considered as strong states.

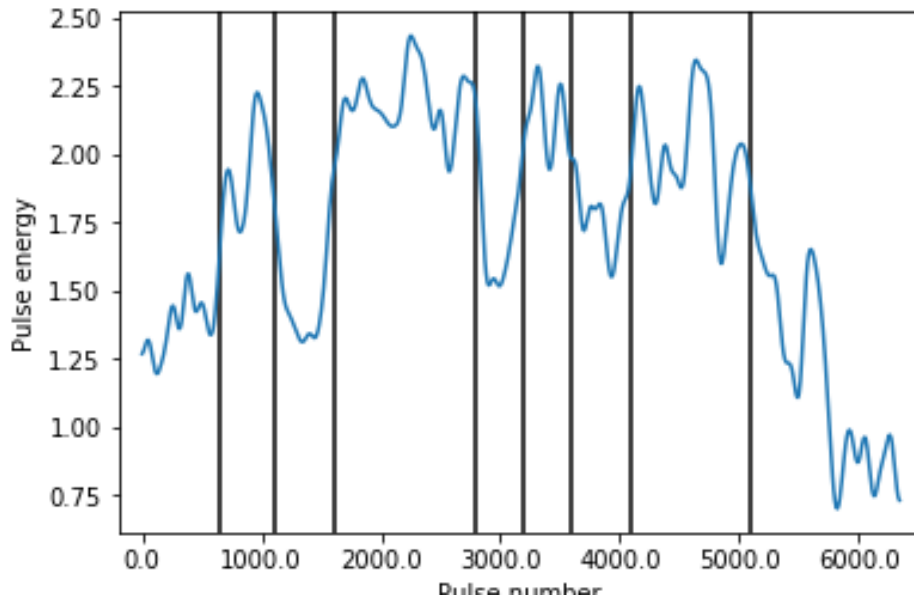


Figure 4.17: Pulse energy vs pulse number trend for epoch II resulting from convolution with Gaussian filter. Here the high and the low pulse strength regions are shown with divisions using the black vertical lines.

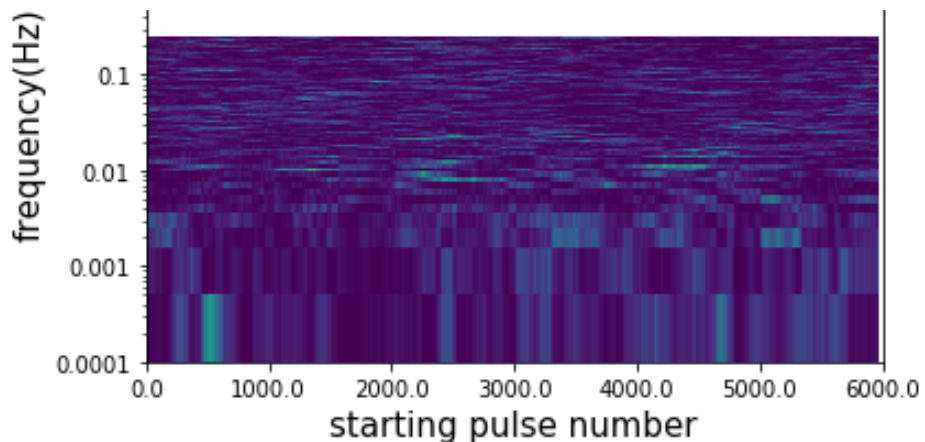


Figure 4.18: Sliding FFT method applied to the non-stationary pulse energy vs. pulse number series for epoch II.

Now the series in Figure 4.13 being a non-stationary time series, dynamic sliding FFT technique can be used to verify if any underlying periodicity is present. The result is presented in Figure 4.18. This time candidates for possible significant modulation were observed at different pulse numbers such as 1000-1500, 2000-2300, 2200-3500, and 4000-4400 with frequency

0.011 Hz, 0.033 Hz, 0.007 Hz, and 0.0136 Hz respectively. When these regions were checked using conventional Fourier transform, non-identical frequencies were revealed. So again there was mismatch of frequencies observed at those particular pulse numbers. The observed modulations were present only for a brief period of time, which indicates that even if modulations exist, they might be transient in nature.

Finally, it was examined whether the presence of modulations observed in sliding FFT of epoch II was dependent on the aforementioned strong and weak states. We observed that the modulation candidates were equally present in strong states as well as the weak states.

4.7.3 Pulse energy distribution

Pulse energy was represented by the area under 'on' pulse region and gives an estimate of the strength of each pulse. To get a statistical quantification of range of the pulse energy variation in two epochs, 'on' pulse energy and 'off' pulse energy were calculated and plotted as shown in Figure 4.19 and Figure 4.20 for epoch I and epoch II respectively.

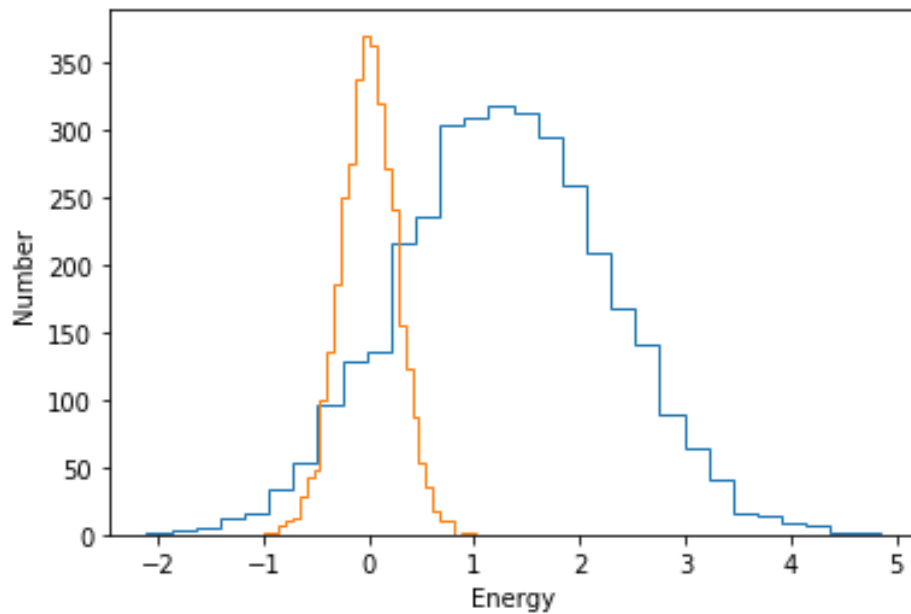


Figure 4.19: ON (blue curve) and OFF (orange curve) pulse energy distribution of PSR J1825–0935 for epoch I

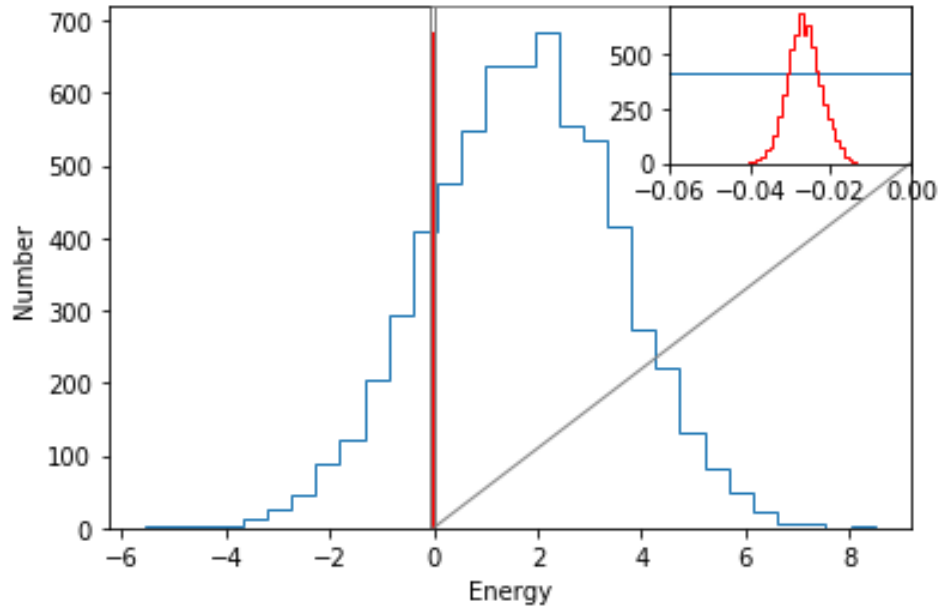


Figure 4.20: ON (blue) and OFF (red) pulse energy distribution of PSR J1825-0935 for whole epoch II. The inset shows zoomed off pulse energy distribution. The variation on the on pulse distribution is significantly higher than the variation of the off pulse distribution in this case compared to epoch I.

The blue line curve represents the energy under 'on' pulse region, whereas the other curve represents the energy under 'off' pulse region in Figure 4.19 and Figure 4.20 for the two epochs of observation. In case of normal non-nulling pulsars, little overlap is seen between on pulse and off pulse energy distributions. Here, however, we see significant overlap between the two distributions for both epochs (significant nulls had not been previously reported for this pulsar). The significant overlapping of the on and off pulse energy distributions might indicate the presence of nulling, however more sensitive observations are required to confirm this phenomenon. In general, for this low frequency observation the on pulse energy distribution shifted towards lower pulse energies (possibly due to the telescope sensitivity at this low frequency) compared to higher frequency observations [15], which may also result in the observed overlap. And also from these plots, we can compare between global energy distribution and average pulse energy between two epochs. The wider energy distribution

of the on pulse energy in epoch II compared to epoch I is consistent with the global pulse energy variation as observed in Figure 4.17. This further emphasizes the time evolution of pulsar emission properties and strong time-dependence of the pulsation modulation of PSR J1825–0935 .

4.7.4 Polarisation analysis

Polarisation studies of PSR J1825–0935 were performed for epoch I for 270 pulses as shown in Figure 4.21 which shows the pulse profile for epoch I in each of the I, Q, U, and V modes. It is clear from the plot that emission was dominant in linear polarisation mode (Q), and the central part of the pulse showed lower circular polarisation (V) than the trailing and leading parts.

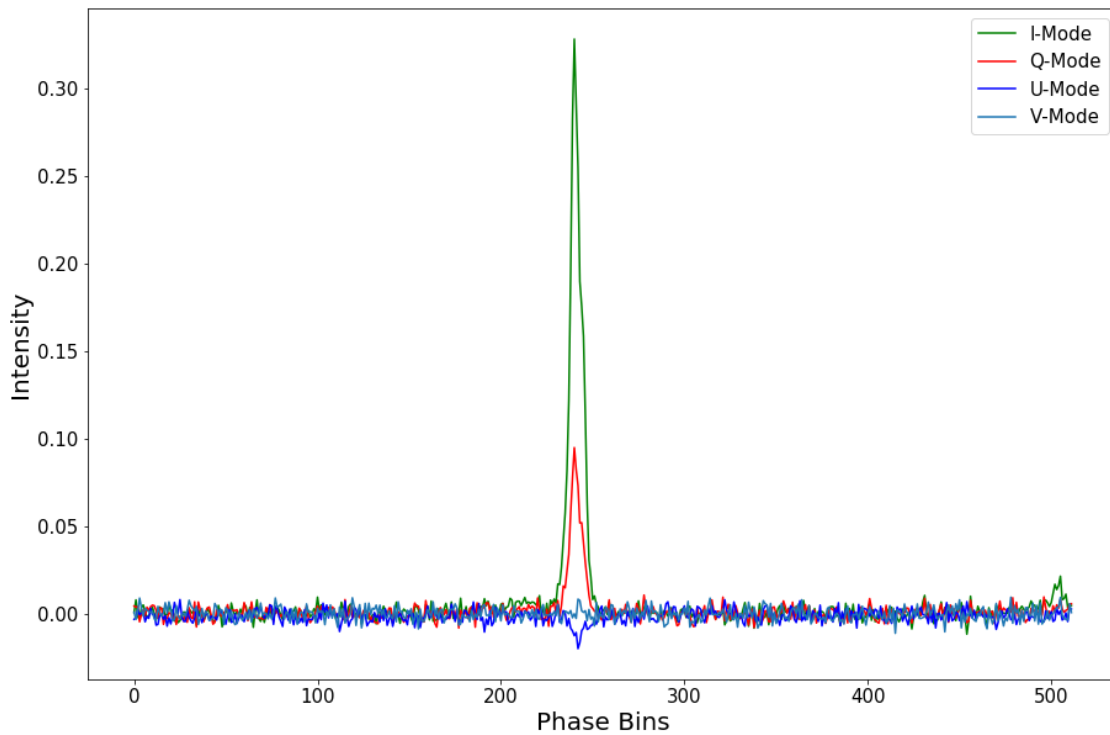


Figure 4.21: Polarisation profile of PSR J1825–0935 for a section of epoch I

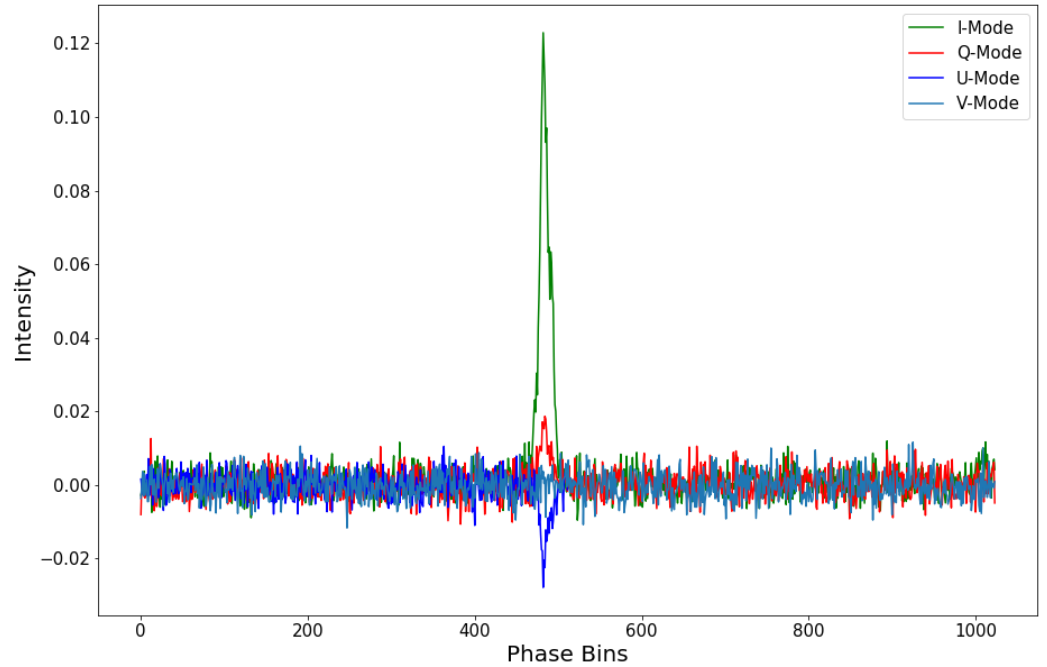


Figure 4.22: Polarisation profile of PSR J1825–0935 for whole epoch II

Similar analysis was done for epoch II for 6500 pulses as shown in Figure 4.22 which shows the pulse profile for epoch II in each of the I, Q, U, and V modes. A similar behavior to epoch I, i.e., relatively low circular polarisation for the pulse center compared to trailing and leading parts, was observed. However, in this case the circular polarization (V) displayed a more negative value, possibly due to a higher exposure time for epoch II relative to epoch I.

Chapter 5

Discussion and conclusion

We carried out a detailed pulse and single-pulse studies of PSR J1825–0935 using MWA observations at a low frequency of 184.96 MHz. This work investigates the pulsation properties and the periodic amplitude modulation characteristics of PSR J1825–0935 at low frequencies with unprecedented sensitivity.

On plotting the averaged pulse profile for 3500 s of observation time in epoch I and for 6500 s of observation time in epoch II, a clear main peak was obtained, but there was also a hint of interpulse in the profile. The weak nature of the interpulse may be due to weaker strength of interpulse at such low frequencies or in this particular state of time of the pulsar interpulse has become weak. It may be likely that we are observing PSR J1825–0935 in the Q-mode (quiet-mode) [1].

Plotting the calculated pulse energy of the sub-pulses against pulse number clearly showed variation in the pulse energy. This indicated towards the presence of periodic amplitude modulation of the pulses. As we have seen earlier, non-zero value of modulation index implies the presence of different levels of variation within ON pulse region. We observed that the trailing part of the PSR J1825–0935 pulse showed more intensity modulation than leading part of the pulse in the epoch I, whereas in epoch II, it showed opposite behavior, i.e., leading part of the main pulse showed more modulation index than the trailing part. The study of the same phenomenon at 1369 MHz for the same pulsar showed more intensity modulation in the leading part of the

pulse [1] than the trailing part (which is consistent with our epoch II result. Detailed timing analysis showed transient candidates for pulse amplitude modulation at certain frequencies within specific pulse ranges of the pulse train. These show that amplitude modulation phenomena is a time-evolving phenomenon. Further the observed non-dependence of the presence of modulation candidates on strong or weak states in this work, might help set a constraint on emission mechanisms behind them, indicating that the two origin processes may be uncorrelated. The variation in the magnetospheric currents that may be responsible for the amplitude modulation [28], is most probably not directly related to the physical phenomenon governing the enhancement of the pulse strength resulting in the strong and weak states. This needs to be investigated further as this can have important consequences for the emission process and geometry and the spectral nature of the pulse and its micro-structures. As seen in the fluctuation spectra section, detection sensitivity is insufficient to determine the periodic nature of modulation. Further high sensitive observations are required to get more conclusions regarding the emission processes and beam geometry. No polarisation position angle plots and estimates on the magnetospheric geometry analysis was done for PSR J1825–0935 earlier, similar to the ones mentioned in [34], and strong limits on the beam geometry could not be presently given from the polarization profile analysis.

Similar studies were done for pulsar B1929+10 at various frequencies [22, 23]. When observations were studied and analysed at 333 MHz using GMRT, periodic amplitude modulation was seen with a period of $11.5 \pm 1.3 P$ and no sub pulse drifting was observed [15, 20]. At 1.5GHz only modulation features were observed, no drifting pattern was observed [32]. The comparative description of the modulation parameters of a selected sample of pulsars is shown in Figure 5.1 taken from [25]. Here P , \dot{P} , P_3 , and \dot{E} are the spin period, spin-down rate, modulation periodicity, and spin-down energy of the pulsar respectively. PSR J1825–0935 is given in the third row, with the spin-down energy highlighted. The \dot{E} is higher for this pulsar than the empirical threshold of 2×10^{32} erg/s that is required for pulsars to exhibit pulse amplitude modulation [1]. This pulsar showed a relatively higher modulation periodicity in previous works [1, 28], however in this work, we

obtained modulation candidates at relatively lower modulation periodicities. The pulsars with phase lock (between Interpulse and Mainpulse) were tending to show relatively higher energy loss states. For PSR J1825–0935, however we could not observe any such phase locking behavior possibly owing to the extremely weak presence of the Interpulse.

Table 2. The (modulation) parameters of PSRs B1055-52, B1702-19, B1822-09 and B1929+10.

PSRB	P	\dot{P} (10^{-15})	P_3	\dot{E} (10^{33})	P_{delay}	τ_{delay}
	s	s/s	P	erg/s	P	s
1055-52	0.197	5.83	21 ± 2^a	30	2.5^a	0.49
1702-19	0.299	4.14	11 ± 0.4^b	6.1	0.5^b	0.15
1822-09	0.769	52.5	43 ± 1^c	4.5	—	—
1929+10	0.227	1.16	12 ± 1	3.9	1	0.23

Figure 5.1: The pulse amplitude modulation parameters of pulsars B1055-52, B1702-19, B1822-09, and B1929+10 [1, 31, 32]. This table was taken from [25].

The dependence of the periodic amplitude modulation and sub pulse drifting on frequency is still an unclear phenomenon. Our work sheds light on the observational behavior of this phenomenon at low frequencies, which can be essential in understanding the radiative behavior and the emission characteristics of amplitude modulation observed in pulsar radiation. We observed that modulation phenomena might be a transient phenomenon. Additionally, given that this feature was often strongly prevalent at other frequencies, pulse amplitude modulation might also be quite a frequency dependent phenomenon. We were able to constrain the high energy and low energy states emission mechanism being uncorrelated to the emission mechanism responsible for modulation phenomenon. Modulation index was also found to vary with time. Linear polarisation was appearing to be dominant than circular polarisation, implying that curvature radiation might be the responsible one for the observed behavior. However, synchrotron emission with favourable geometry may also be responsible. With upcoming

highly sensitive telescopes, these phenomena can be studied in great detail, possibly provide us greater understanding of the physical processes occurring in pulsars.

Chapter 6

Future Plans

In further research:

1. We plan to extend this analysis to the other two MWA observations at different epochs separated by time. We plan to examine the time evolution of single-pulse properties, especially that of the periodic amplitude modulation. Our results already indicate that this feature is highly dependent on time. Such an extensive study over multiple epochs will help constrain the physical factors triggering the amplitude modulation mechanism.
2. Searches for interpulse, precursor and different pulsation modes will also be carried out over the data of the different epochs.
3. Compare the results obtained with similar amplitude modulation feature for other times, frequencies and sources.
4. Due to mode changing behavior exhibited by PSR J1825–0935 , pulsar beam geometry and emission mechanisms can be studied in more detailed manner by geometric and polarimetric analysis [34].

References

1. W. M. Yan, R. N. Manchester, N. Wang, J. P. Yuan Z. G. Wen and K. J. Lee, 2019, MNRAS, 485, 3242, 3245
2. Jenet F.A., Anderson S.B, and Prince T.A, 2000, ApJ, 546, 395
3. Basu, Mitra & Melikidze., 2019, ApJ, 889, 133
4. Bhattacharyya B., Gupta Y., Gil J., 2010, MNRAS, 408, 407
5. Lorimer, Living Reviews in Relativity, 2005, Article 7
6. ATNF catalogue (<https://www.atnf.csiro.au/research/pulsar/psrcat/>)
7. DSPSR (<http://dpsr.sourceforge.net/index.shtml>)
8. MWA (<https://www.mwatelescope.org/>)
9. Hand book of Pulsar Astronomy, D.Lorimer and M. Kramer
10. Pulsars (<http://www.jb.man.ac.uk/distance/frontiers/content.htm>)
11. PRESTO (<https://www.cv.nrao.edu/~sransom/presto/>)
12. van Straten, W., Bailes, M., 2011, Publ. Astr. Soc. Aust., 28, 2
13. Hotan, A. W., van Straten, W., Manchester, R. N., 2004, Publ. Astr. Soc. Aust., 21, 303
14. PSRCHIVE (<http://ipta.phys.wvu.edu/files/student-week-2018/rms-pulsar-psrchive.pdf>)
15. Basu, R., Mitra, D., Melikidze, G.I., & Skrzypczak, A., 2019a, MNRAS, 482, 3757

16. Backer D.C., 1970, *Nature*, 227, 292
17. Biggs J.D., 1992, *ApJ*, 394, 574
18. Ritchings R.T., 1976, *MNRAS*, 176, 249
19. Ruderman M.A & Suderland P.G., 1975, *ApJ*, 196, 51
20. Basu R., Mitra D., Melikidze G. I., Maciesiak K., Skrzypczak A., Szary A., 2016, *ApJ*, 833, 29
21. Lyne A., Hobbs G., Kramer M., Stairs I., Stappers B., 2010, *Science*, 329, 408
22. P. Weltevrede, B. W. Stappers, R. T. Edward, 2007, *A&A*, 445, 243
23. Backer, D. C. 1973, *ApJ*, 182, 245
24. Rankin, J. M., & Rathnasree, N. 1997, *Journal of Astrophysics and Astronomy*, 18, 91
25. F. F. Kou, W. M. Yan, B. Peng, J. G. Lu, K. Liu, C. M. Zhang, R. G. Strom, L. Wang, J. P. Yuan, Rai Yuen, Y. Z. Yu, J. M. Yao, B. Liu, J. Yan, P. Jiang, C. J. Jin, D. Li L. Qian, Y. L. Yue, Y. Zhu, and (The FAST collaboration), *ApJ*, 2021, 909, 170.
26. Force, M.M.; Rankin, J.M. 2010, *MNRAS*, 406, 237
27. Fowler L. A., Wright G. A. E., 1982, *A&A*, 109, 279
28. Latham C., Mitra D., Rankin J., 2012, *MNRAS*, 427, 180
29. Hermsen W., et al., 2017, *MNRAS*, 466, 1688
30. Lyne A., Hobbs G., Kramer M., Stairs I., Stappers B., 2010, *Science*, 329, 408
31. Mitra, D.; Arjunwadkar, M.; Rankin, J. 2015, *ApJ*, 806, 236
32. Weltevrede, P., Wright, G. A. E., & Stappers, B. W. 2007, *A&A*, 467, 1163
33. Weltevrede, P., Wright, G., & Johnston, S. 2012, *MNRAS*, 424, 843

34. Brinkman, Casey Lynn, "Polarization and Pulsars" (2017). UVM College of Arts and Sciences College Honors Theses. 41.
35. Gil, J.; Melikidze, G.I.; Geppert, U. 2003, A&A, 407,315
36. Szary, A.; Melikidze, G.I.; Gil, J. 2015,MNRAS, 447,2295